Decay rates and decoherence of an interstitial two-level spin impurity in a ferromagnetic lattice

Yamen Hamdouni ⬤[*]

Department of physics, Faculty of Exact Sciences, Mentouri University, Constantine, Algeria

The decay rate of an interstitial two-level spin impurity, located in the center of a unit cell of an anisotropic ferromagnetic lattice subjected to an external magnetic field, is derived. The impurity is coupled to nearest-neighbor spins through a Heisenberg *XY* interaction. By mapping the lattice spin operators using the Holstein-Primakoff transformation, we establish the similarity with the Fano-Anderson model at low temperatures, and we calculate the retarded Green's function in one and two dimensions analytically for arbitrary coupling strength. It is shown that the reduced density matrix of the impurity satisfies an exact master equation in Lindblad form, from which the decay rate and the Lamb shift are deduced. The evolution in time of the latter together with the excited-state occupation probability is investigated and its dependence on the applied magnetic field is discussed. It is found that there exists a critical resonance-like value of the magnetic field around which the behavior of the decay rate and the density matrix changes drastically. The Markovian decay law, as given by the Fermi golden rule, does not hold in the weak-coupling regime unless the magnetic field is weak, typically less than the critical value. The weak-coupling regime is further treated perturbatively up to second order, and the obtained results are compared with the exact solution. We also discuss the Zeno regime of the dynamics, where it is shown that, at short times, the effective decay rate is twice as small as the exact decay rate, and that when the impurity energy lies outside the lattice continuum, the measurement speeds up the decay of the survival probability.

I. INTRODUCTION

The complete description of the dynamics of (small) quantum systems should take into account the influence of the surrounding environment on the different features of their evolution. This represents the basic concept behind the theory of open quantum systems [1]. As a matter of fact, many interesting phenomena cannot be explained in a plausible way without the inclusion of the effect of the outer environment. The prominent examples that attracted much attention include decoherence, dephasing, and dissipation phenomena, to name a few [2–4]. Apart from their fundamental relevance in the development of quantum mechanics, these processes are of great importance in many applications, ranging from nuclear physics to quantum optics.

Very often, the properties of the environment, which *a priori* is characterized by a large number of degrees of freedom, make it very difficult, if not impossible, to solve in an exact manner the evolution equations. Fortunately, there exist systems of great practical relevance for which the dynamics can be exactly solved. For instance, the Jaynes-Cummings model [5] represents one of the most popular and important paradigms that enabled the investigation of the dynamics of open quantum systems. It has been widely used in many contexts and it is of great usefulness, both theoretically and experimentally. Depending on whether the environment is of bosonic or of fermionic nature, many techniques have been proposed in order to eliminate the irrelevant environment degrees of freedom [6–17]. Generally speaking, in the

bosonic case, this task is achieved through the introduction of a spectral density for the system-environment coupling (usually of Lorentzian form), along with the so-called Born and Markovian approximations. The latter is widely used in, e.g., quantum optics, and is based on the assumptions that the characteristic timescale of the environment is much smaller that that associated with the central system. This leads to a loss of memory of the system, which is generally associated with Markov processes. As a consequence, the reduced system density matrix is found to satisfy a master equation which is in the Lindblad form. The latter is characterized by decay rates which are essentially positive and time-independent.

However, the validity of the Markovian approximation is not justified in many systems that display features indicating strong non-Markovian behavior. This is, for example, the case when the decay rates become negative, implying that information flows back from the environment to the system; consequently, the memory effects should be taken into account even for weak coupling. Actually, the non-Markovian dynamics of quantum systems became over the last years one of the most interesting subjects in the theory of open quantum systems [18–20]. This is mainly due to the lack of an exact general non-Markovian master equation, in contrast with the known Lindblad form of the Markovian dynamics.

The Fano-Anderson model describes a single discrete state or impurity that is coupled to a continuum of states. It was first introduced by Fano [21] and Anderson [22] to study magnetic impurities in metals. Notice that the impurity spin models are often met in the field of solid-state physics, where the continuum may refer, for example, to an electron gas [23,24]. This model, among other paradigms, has been

_____
*hamdouniyamen@gmail.com

the main tool in approaching various physical problems such as the spontaneous emission in dielectrics and photonic crystals, charge transfer in one-dimensional semiconductors, the Bose-Einstein condensate, and the decay in Josephson junctions [25–43]. Recently, the general non-Markovian dynamics of open systems has been investigated via the use of Green's function for systems linearly coupled to thermal environments by Zhang *et al.* [34]. They used a model similar to the Fano-Anderson one and showed how the exact master equation may be derived. In most investigations, the spectral densities of the environments studied are defined over an infinite domain of mode frequencies where a frequency cutoff is introduced. Generally speaking, the exponential Markovian decay occurs for weak system-environment coupling [44]. In Ref. [25], the authors report on an oscillatory variation of the decay of the spontaneous emission of a two-level atom coupled to a radiation field whose spectrum possesses band gaps. The decay of the population on the excited state displays mostly non-Markovian dynamics for small detuning from the atomic resonant frequency. For large detuning, the decay becomes nearly Markovian (exponential); the same behavior has been reported in Ref. [27].

In this paper, we focus on the study of the non-Markovian dynamics of a central spin impurity that is coupled to a ferromagnetic spin lattice. The latter presents periodic properties [45,46] that fix in a unique manner the spectral density. It should be stressed that the spin degrees of freedom are the most suitable candidates towards the implementation of new quantum technologies [47,48]. One can, for instance, profit from their properties to implement the proposed quantum algorithms [49–54]. In this work, we shall be mainly interested in the decay rates, whose properties determine the way the reduced density matrix behaves in time.

The paper is organized as follows. In Sec. II we introduce the total Hamiltonian of the composite system. Then, through the Holstein-Primakoff transformation, we use the spin-wave theory to establish the connection with the Fano-Anderson model. Section III deals with the study of the dynamics of the impurity at zero temperature, where analytical results for one and two dimensions are presented, and the evolution of the decay rate and the occupation probability is discussed. Section IV is devoted to the study of the weak-coupling regime where we use the second-order perturbation theory to derive the master equation for the reduced density matrix, and we compare the results with the exact solutions. There, the short-time evolution is discussed in more detail. In Sec. V we investigate the quantum Zeno effect. We end the paper with a brief conclusion.

II. MODEL

A. System Hamiltonian

Consider a two-level localized spin impurity that is immersed in a ferromagnetic spin lattice in d dimensions. The impurity is dealt with as a central open system, while the lattice plays the role of the spin bath. The total model Hamiltonian H is given by the sum of three terms: the free Hamiltonian of the central system, which we designate by H_S, the Hamiltonian of the lattice H_B, and the interaction Hamiltonian H_{SB} describing the coupling of the impurity to

the spins of the lattice. Therefore, we can write

$$H = H_S + H_B + H_{SB}. \qquad (1)$$

The free Hamiltonian of the two-level system may be expressed in terms of the usual Pauli matrices as

$$H_S = \omega_0 \sigma_+ \sigma_-, \qquad (2)$$

where ω_0 is the energy gap between the ground state and the excited state of the impurity. Note that the formalism we use applies as well to the case of a qubit where the free Hamiltonian is written as $H_S = (\omega_0/2)\sigma_z$, ω_0 being proportional to the strength of the local magnetic field applied to the qubit.

The lattice is subject to the effect of a homogeneous magnetic field, applied along the z direction, the strength of which is denoted by h. The Hamiltonian describing the lattice reads

$$H_B = -\sum_{\langle i,j \rangle} \left(J_{i,j}^x S_i^x S_j^x + J_{i,j}^y S_i^y S_j^y + J_{i,j}^z S_i^z S_j^z \right) - h \sum_j S_j^z, \qquad (3)$$

where S_i^x, S_i^y, and S_i^z represent the components of the spin operator of the spin of magnitude S located at site i. In the above equation, the summation is performed with respect to all pairs of spins. The parameters $J_{i,j}^x$, $J_{i,j}^y$, and $J_{i,j}^z$ denote the coupling constants, which are all positive. We assume that the lattice is of XXZ type and that each spin interacts only with its nearest neighbors, whose number is denoted from here on by η (the coordination number).

Under the above assumptions, the lattice Hamiltonian can be written as

$$H_B = -J \sum_{j\delta} \left(S_j^x S_{j+\delta}^x + S_j^y S_{j+\delta}^y + \gamma_z S_j^z S_{j+\delta}^z \right) - h \sum_j S_j^z, \qquad (4)$$

where δ designates the d-dimensional vectors joining each spin at a given site to its nearest-neighbor spins, and $J = J_{i,i+\delta}^x = J_{i,i+\delta}^y$ denotes the coupling constant restricted to these neighbors, whereas $\gamma_z = J_{i,i+\delta}^z/J$ is the anisotropy parameter which satisfies $\gamma_z \geqslant 1$. This easy-axis condition ensures that the lattice is in the ferromagnetic phase, where the ground state is the one in which all the spins are directed along the z direction. At this stage, it is useful to introduce the raising and lowering operators $S_j^{\pm} = S_j^x \pm iS_j^y$, which enables us to rewrite the lattice Hamiltonian in the form:

$$H_B = -\frac{J}{2} \sum_{j\delta} \left[(S_j^+ S_{j+\delta}^- + S_j^- S_{j+\delta}^+) + 2\gamma_z S_j^z S_{j+\delta}^z \right] - h \sum_j S_j^z. \qquad (5)$$

We further assume that the coupling between the spin impurity and the lattice is of Heisenberg XY type, whose Hamiltonian is given explicitly by the formula

$$H_{SB} = \sum_j (g_j \sigma_- S_j^+ + g_j^* \sigma_+ S_j^-), \qquad (6)$$

where g_j denotes the coupling constant of the central system to the spin located at site j; for the sake of generality, we assume it to be complex-valued.

B. Spin-wave formulation

The properties of ferromagnets at low temperatures can be investigated by means of the spin-wave theory, where the concept of the magnon naturally arises as the analog of the photon in electromagnetic radiation and of the phonon for the lattice vibrations. Generally speaking, magnons are ground-state excitations that propagate through the spin lattice as a result of thermal or quantum perturbations. The standard method in spin-wave theory consists in using suitable transformations that map the spin operators to bosonic operators. In this work we use the Holstein-Primakoff transformation which proved to be very convenient in solving such problems. Recall that the prescription employed in the Holstein-Primakoff transformation resides in the following identities [55]:

$$S_j^- = \sqrt{2S}\sqrt{1 - \frac{b_j^\dagger b_j}{2S}}b_j, \quad S_j^+ = \sqrt{2S}b_j^\dagger\sqrt{1 - \frac{b_j^\dagger b_j}{2S}}, \quad (7)$$

$$S_j^z = S - b_j^\dagger b_j, \quad (8)$$

where b_j are bosonic operators that satisfy $[b_j, b_{j'}^\dagger] = \delta_{jj'}$.

At low temperatures, the mean number of magnons is very small; therefore, by expanding the square root in Eq. (7) in a Taylor series and keeping only bilinear terms in b_j and $b_j^\dagger$ in the Hamiltonian of the lattice, it follows that

$$H_B = -JS\sum_{j\delta}[(b_j^\dagger b_{j+\delta} + b_j b_{j+\delta}^\dagger) + 2\gamma_z(b_j^\dagger b_j + b_{j+\delta}^\dagger b_{j+\delta})]$$

$$+ h\sum_j b_j^\dagger b_j - hNS - J\eta\gamma_z NS^2, \quad (9)$$

where N is the number of sites or spins in the lattice. Next, we Fourier transform the bosonic operators b_j as follows:

$$b_j = \frac{1}{\sqrt{N}}\sum_{\vec{k}} e^{i\vec{k}\cdot\vec{r}_j}a_{\vec{k}}, \quad a_{\vec{k}} = \frac{1}{\sqrt{N}}\sum_j e^{-i\vec{k}\cdot\vec{r}_j}b_j, \quad (10)$$

where $\vec{r}_j$ designates the d-dimensional real-space vector that determines the position of the spin at site j of the lattice. It can easily be verified that the operators $a_{\vec{k}}$ satisfy $[a_{\vec{k}}, a_{\vec{k}'}^\dagger] = \delta_{\vec{k}\vec{k}'}$. By virtue of Eq. (10), the lattice Hamiltonian is written as

$$H_B = \sum_{\vec{k}}(h + 2J\gamma_z\eta S - J\eta S2\tau_{\vec{k}})a_{\vec{k}}^\dagger a_{\vec{k}} - hNS$$

$$- J\eta S/2\sum_{\vec{k}}\tau_{\vec{k}} - J\eta\gamma_z NS^2, \quad (11)$$

where

$$\tau_{\vec{k}} = \frac{1}{\eta}\sum_{\vec{\delta}} e^{i\vec{k}\cdot\vec{\delta}} \quad (12)$$

is the lattice structure factor. Hence, we deduce that the dispersion relation is given by

$$\Omega_{\vec{k}} = h - 2J\eta S(\tau_{\vec{k}} - \gamma_z). \quad (13)$$

This implies that the spectrum of the lattice corresponds to the energy domain $\Omega_{\vec{k}} \in [\Omega_{\min}, \Omega_{\max}]$, with $\Omega_{\min} = h + 2J\eta S(\gamma_z - 1)$ and $\Omega_{\max} = h + 2J\eta S(1 + \gamma_z)$ (we set $\hbar = 1$).

In a similar way, it can be shown that the interaction Hamiltonian H_{SB} may be expressed in terms of the bosons

operators as

$$H_{SB} = \sum_{\vec{k}}(g_{\vec{k}}\sigma_- a_{\vec{k}}^+ + g_{\vec{k}}^*\sigma_+ a_{\vec{k}}), \quad (14)$$

where the new coupling constant $g_{\vec{k}}$ is defined through the expression:

$$g_{\vec{k}} = \sqrt{\frac{2S}{N}}\sum_j g_j e^{i\vec{k}\cdot\vec{r}_j}. \quad (15)$$

Clearly, the latter form of the coupling constant depends on the position of the impurity, as well as on the dimension and type of lattice.

III. EXACT DYNAMICS AT ZERO TEMPERATURE ($T = 0$)

The evolution in time of the state of the spin impurity at zero temperature can be exactly derived. We begin with the one-dimensional lattice where we present the main calculations and procedures, which are of general applicability and hold at higher dimensions; afterwards, we deal with the two-dimensional case where we show that the dynamics can also be investigated analytically.

A. One-dimensional lattice

The dynamics in one dimension bears a particular importance as certain interesting features arise, which are absent in two and three dimensions. The lattice in this case is a one-dimensional array of spins, the length of which is given by $(N - 1)\delta$, where δ represents the distance separating two adjacent sites. The wave vector has only one component k, and the first Brillouin zone corresponds to the interval $-\pi/\delta \leqslant k \leqslant \pi/\delta$. We assume that the impurity lies in the middle between two lattice spins and that it interacts only with these two neighbors, with coupling constant g. The nonlocal coupling constant $g_{\vec{k}}$ is thus given by

$$g_{\vec{k}} = 2g\sqrt{\frac{2S}{N}}\cos\left(\frac{\delta k}{2}\right). \quad (16)$$

Next, we introduce the retarded Green's function of the impurity which is given by

$$G_{\text{ret}}(\epsilon) = \frac{1}{\epsilon - \omega_0 - \Sigma_{\text{ret}}(\epsilon + i\nu)}, \quad (17)$$

where $\Sigma_{\text{ret}}(\epsilon + i\nu)$ is the retarded self-energy, namely:

$$\Sigma_{\text{ret}}(\epsilon + i\nu) = \sum_k \frac{|g_{\vec{k}}|^2}{\epsilon - \Omega_k + i\nu}, \quad (18)$$

with ν being an infinitesimal positive quantity. It should be stressed that, due to the XY coupling of the impurity to the lattice, the only self-energy diagram after bosonization is the one obtained in the second-order expansion of the S matrix with respect to the coupling constants $g_{\vec{k}}$, in analogy with the Fano-Anderson model. Hence the Green's function (17) is actually an exact one that is obtained by summing all the

diagrams, which amounts to writing [23]

$$G(\epsilon) = G_0(\epsilon) + G_0(\epsilon)\Sigma(\epsilon)\left[G_0(\epsilon) + G_0^2(\epsilon)\Sigma(\epsilon) + \cdots\right]$$
$$= \frac{G_0(\epsilon)}{1 - G_0(\epsilon)\Sigma(\epsilon)}, \tag{19}$$

where $G_0(\epsilon) = (\epsilon - \omega_0)^{-1}$ is the Green's function of the free impurity, and $\Sigma(\epsilon)$ is the self-energy.

In the limit $N \to \infty$, the number of modes becomes very large, and hence the spectrum of the lattice turns into a continuum of states, whose energies are bounded between $h + 4JS(\gamma_z - 1)$ and $h + 4JS(\gamma_z + 1)$. In this limit, in d dimensions, the sum with respect to the wave vector $\vec{k}$ may be replaced with an integral over the first Brillouin zone (FBZ)

according to the rule

$$\frac{1}{N}\sum_{\vec{k}} \to \frac{v_d}{(2\pi)^d}\int_{FBZ} d\vec{k}, \tag{20}$$

where v_d is the volume of a unit cell. Consequently, by virtue of Eq. (16), the retarded self-energy can be expressed as

$$\Sigma_{\text{ret}}(\epsilon + i\nu) = \frac{4g^2S}{\pi}\int_{-\pi}^{\pi}\frac{\cos^2(k/2)dk}{\epsilon - h - 4JS\gamma_z + 4JS\cos(k) + i\nu}. \tag{21}$$

By the change of variable $z = e^{ik}$, the above integral is transformed into a contour integral around the unit circle, so the theorem of residues can be applied. It follows that the real part of the self-energy reads

$$\text{Re }\Sigma_{\text{ret}}(\epsilon + i\nu) = \begin{cases} \frac{g^2}{J}\left(1 - \sqrt{\frac{\epsilon - h - 4JS\gamma_z - 4JS}{\epsilon - h - 4JS\gamma_z + 4JS}}\right) & \text{for } 4JS \leqslant |\epsilon - h - 4JS\gamma_z| \\ \frac{g^2}{J} & \text{for } 4JS > |\epsilon - h - 4JS\gamma_z|. \end{cases} \tag{22}$$

On the other hand, the imaginary part can be calculated when $\nu \to 0^+$ as

$$\text{Im }\Sigma_{\text{ret}}(\epsilon + i0^+) = -\frac{g^2}{J}\left(\frac{h - \epsilon + 4JS(1 + \gamma_z)}{\sqrt{(4JS)^2 - (\epsilon - h - 4JS\gamma_z)^2}}\right) \text{ for } 4JS > |\epsilon - h - 4JS\gamma_z|, \tag{23}$$

and $\text{Im }\Sigma_{\text{ret}}(\epsilon + i0^+) = 0$ for $4JS < |\epsilon - h - 4JS\gamma_z|$. This actually reflects the fact that the imaginary part of the retarded self-energy vanishes outside the continuum, namely, $\text{Im }\Sigma_{\text{ret}}(\epsilon + i\nu) = 0$ for $\epsilon > \Omega_{\max}$ or $\epsilon < \Omega_{\min}$.

The fundamental property exhibited by the retarded Green's function is that the spectral density $A(\epsilon)$ is related to the former through the identity

$$A(\epsilon) = -2\,\text{Im }G_{\text{ret}}(\epsilon). \tag{24}$$

The spectral density represents essentially the probability that the impurity has energy ϵ as a result of its coupling to the lattice. Inside the continuum, it can be expressed as

$$A(\epsilon) = -\frac{2\,\text{Im }\Sigma_{\text{ret}}(\epsilon + i0^+)}{[\epsilon - \omega_0 - \text{Re }\Sigma_{\text{ret}}(\epsilon + i0^+)]^2 + [\text{Im }\Sigma_{\text{ret}}(\epsilon + i0^+)]^2}. \tag{25}$$

Outside the continuum, that is when $\text{Im }\Sigma_{\text{ret}}(\epsilon + i0^+) \to 0$, the spectral density reduces to

$$A(\epsilon) = 2\pi\delta[\epsilon - \omega_0 - \text{Re }\Sigma_{\text{ret}}(\epsilon + i0^+)]$$
$$= 2\pi\sum_j\frac{\delta(\epsilon - \epsilon_j)}{1 - \frac{d}{d\epsilon}\text{Re }\Sigma_{\text{ret}}(\epsilon + i0^+)|_{\epsilon_j}}, \tag{26}$$

where ϵ_j are the solutions of the equation $\epsilon - \omega_0 - \text{Re }\Sigma_{\text{ret}}(\epsilon + i0^+) = 0$. They may be interpreted as the energies corresponding to localized bound states outside the continuum. Thus, these states are determined in the one-dimensional case by solving the equation:

$$\epsilon - \omega_0 = \frac{g^2}{J}\left(1 - \sqrt{\frac{\epsilon - h - 4JS\gamma_z - 4JS}{\epsilon - h - 4JS\gamma_z + 4JS}}\right) \tag{27}$$

outside the continuum, which can be carried out numerically; however, to gain more insight into the existence of the bound

states, it is convenient to discuss the solutions of the latter equation graphically, as displayed in Fig. 1. It can be shown that there exists always at least one solution no matter what the values of the model parameters are. This is due to the fact that the real part of the self-energy diverges at the lower edge of the spectrum, see Eq. (22). More precisely, the impurity exhibits two bound states whenever $\omega_0 > h + 4JS(1 + \gamma_z) - g^2/J$, otherwise there exists only one bound state. Indeed, from Fig. 1, we see that the value of ω_0 for which the line $y = \epsilon - \omega_0$ passes through the point $(h + 4JS(1 + \gamma_z), g^2/J)$ is given by $h + 4JS(1 + \gamma_z) - g^2/J$; all the values of ω_0
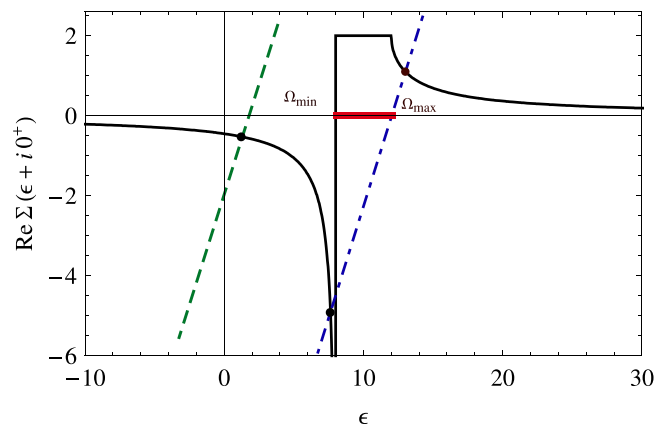

FIG. 1. The real part of the self-energy in one dimension (black solid line) for $J = 0.5$, $g = 1$, $h = 8$, $S = 1$, and $\gamma_z = 1$. The intersection points correspond to the solutions of the equation $\text{Re }\Sigma_{\text{ret}}(\epsilon + i0^+) = \epsilon - \omega_0$ for $\omega_0 = 2$ (green dashed line) and $\omega_0 = 12$ (blue dot-dashed line); these solutions are interpreted in the main text as localized bound states outside the continuum.

exceeding the latter lead to two intersection points outside the continuum.

The retarded Green's function in the time domain is given by the Fourier transform of the spectral density, that is

$$G_{\text{ret}}(t) = -i \int_{-\infty}^{\infty} \frac{d\epsilon}{2\pi} A(\epsilon) e^{-i\epsilon t} = -i\phi_+(t), \qquad (28)$$

where $\phi_+(t)$ is the wave function describing the excited state of the impurity. The integration runs over the full real line to ensure that all the poles of the Green's function outside the continuum are taken into account. In the present model, the range of integration is determined by the energies of the bound states, along with the continuum; at the bound states the spectral density is given by a δ function. Hence,

$$\phi_+(t) = \sum_j \frac{e^{-i\epsilon_j t}}{1 - \frac{d}{d\epsilon} \text{Re}\, \Sigma_{\text{ret}}(\epsilon + i0^+)|_{\epsilon_j}} - \frac{1}{\pi} \int_{\Omega_{\min}}^{\Omega_{\max}} \frac{\text{Im}\, \Sigma_{\text{ret}}(\epsilon + i0^+) e^{-i\epsilon t} d\epsilon}{[\epsilon - \omega_0 - \text{Re}\, \Sigma_{\text{ret}}(\epsilon + i0^+)]^2 + [\text{Im}\, \Sigma_{\text{ret}}(\epsilon + i0^+)]^2}. \qquad (29)$$

Suppose that the initial state of the system is given by the pure state $(\alpha_+|+\rangle + \alpha_-|-\rangle)|\mathcal{G}\rangle$ where $|\mathcal{G}\rangle = \otimes_k |0\rangle_k$ is the ground state of the lattice at $T = 0$. Then, because of the form of the interaction Hamiltonian H_{SB}, the state of the impurity evolves to the mixed one:

$$\rho(t) = \begin{pmatrix} |\alpha_+|^2 |\phi_+(t)|^2 & \alpha_-^* \alpha_+ \phi_+(t) \\ \alpha_- \alpha_+^* \phi_+(t)^* & 1 - |\alpha_+|^2 |\phi_+(t)|^2 \end{pmatrix}. \qquad (30)$$

Differentiating both sides of Eq. (30) with respect to time and using the properties of the Pauli matrices, it can be shown that the above density matrix satisfies the exact master equation

$$\frac{d\rho(t)}{dt} = -i[(\omega_0 + \xi(t)/2)\sigma_+\sigma_-, \rho(t)]$$

$$+ \kappa(t)\left(\sigma_-\rho(t)\sigma_+ - \frac{1}{2}\{\sigma_+\sigma_-, \rho(t)\}\right), \qquad (31)$$

where

$$\kappa(t) = -2\text{Re}\left(\frac{\frac{d}{dt}\phi_+(t)}{\phi_+(t)}\right), \qquad (32)$$

$$\xi(t) = -2\text{Im}\left(\frac{\frac{d}{dt}\phi_+(t)}{\phi_+(t)}\right) - 2\omega_0, \qquad (33)$$

and $\{A, B\}$ denotes the anticommutator of A and B. Physically speaking, the parameter $\kappa(t)$ represents the decay rate of the two-level impurity, while the renormalization parameter $\xi(t)$ plays the role of the Lamb shift due to the coupling to the lattice.

The coupling of the impurity to the neighboring spins depends on the overlap between their wave functions, which fixes the magnitude of the exchange integral g. The overlap depends on the size of the impurity which could, for example, be an atom with one electron in the partially filled shell. Since the impurity is located halfway between two lattice atoms (in the center of a unit cell in general), the exchange between the latter and the impurity can be as strong as the mutual coupling between the lattice constituents. In what follows, we shall consider the strong-coupling as well as the weak-coupling regimes of the dynamics.

An example of the time dependence of the decay rate $\kappa(t)$ and of the Lamb shift $\xi(t)$ is displayed in Figs. 2 and 3 for some particular values of the model parameters. For convenience, the time and the magnetic field h as well as ω_0 are given in units of J. It can be seen that, for strong coupling between the impurity and the lattice, the decay rate takes on larger values as the magnetic field increases until the latter

reaches some yet-to-be-determined critical value (which will be denoted from here on by h_{cri}), above which the decay rate begins to decrease in magnitude. The Lamb shift decreases in turn and after h crosses its critical point the former becomes essentially negative. Another point worth observing is that there appears a peak which is followed by a sharp fall of the decay rate to negative values. This actually happens at times of the order of $1/g$, which clearly is inversely proportional to the
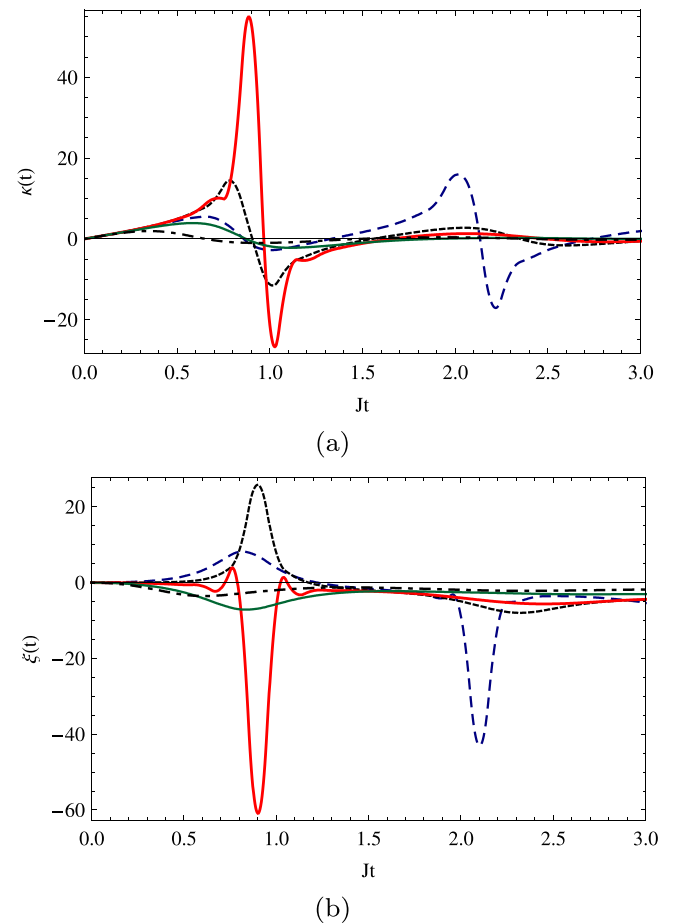

(a)

(b)

FIG. 2. (a) The decay rate κ, and (b) the Lamb shift ξ for strong coupling as a function of time for different values of the strength of the magnetic field: $h = 0.1J$ (blue dashed lines), $h = J$ (black dotted lines), $h = 1.5J$ (red thick solid lines), $h = 3J$ (green thin solid lines), and $h = 4J$ (black dot-dashed lines); other parameters are $\omega_0 = 3J$, $S = 1$, $g = J$, and $\gamma_z = 1$.
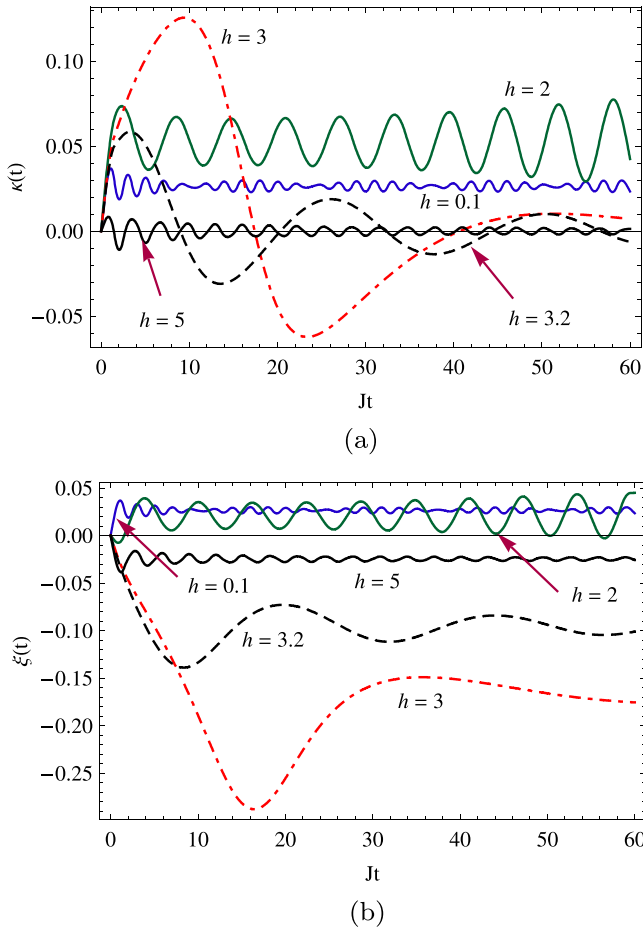
(a)

(b)

FIG. 3. (a) The decay rate κ, and (b) the Lamb shift ξ for weak coupling as a function of time for different values of the strength of the magnetic field (in units of J): $h = 0.1$ (blue solid lines), $h = 2$ (green solid lines), $h = 3$ (red dot-dashed lines), $h = 3.2$ (black dashed lines), and $h = 5$ (black solid lines); other parameters are $g = 0.1J$, $\omega_0 = 3J$, $S = 1$, and $\gamma_z = 1$.

coupling constant. The above results reveal the presence of a critical behavior of the dynamics with respect to the variation of the strength of the applied magnetic field.

It is worthwhile mentioning that the latter evolution features depend in a nontrivial way on the impurity energy. The numerical investigation shows that they take place in the strong-coupling regime ($g \approx J$) only when ω_0 exceeds some threshold value, otherwise the decay rate always decreases as h is raised. Nevertheless, we only assign a critical value to the magnetic field, since, generally speaking, the latter is more accessible from an experimental point of view; this implies that we shall deal with ω_0 as an intrinsic property of the impurity.

Note that, as per the analytical expression of the impurity amplitude $\phi_+(t)$, one cannot *a priori* determine the critical value h_{cri} of the magnetic field. At first sight, it seems to be in connection with the divergence of the self-energy at the lower edge of the lattice spectrum. We carried out many numerical calculations, and we always found that $h_{\text{cri}} < 4JS(1 - \gamma_z) + \omega_0$. Actually, it may be put in the form $h_{\text{cri}} = 4JS(1 - \gamma_z) + \omega_0 - \zeta(g)$, where $\zeta(g)$ is a positive monotonically increasing
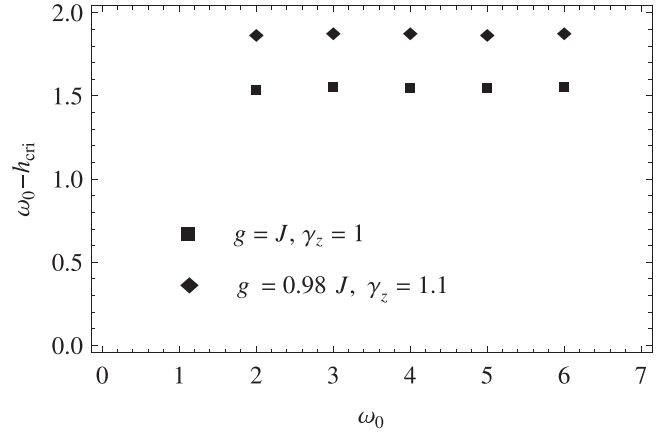

FIG. 4. The numerical estimation of h_{cri} as a function of ω_0 for some values of g and γ_z in the strong-coupling regime. The parameters ω_0 and h_{cri} are given in units of J, and $S = 1$.

function of g. In Fig. 4, we display the numerical estimation of $\omega_0 - h_{\text{cri}}$ as a function of ω_0 for some values of $g \approx J$. The near-constant outcomes suggest the ansatz $\zeta(g) = cg^2/J$, where c is a constant that is approximately equal to $3/2$. The latter yields a good fit to the numerical values, and may be used to locate the vicinity of the critical point for $g \approx J$. A more accurate fit gives $c = 1.56$. Hence, we deduce that, as far as the variation with respect to h is concerned, the critical point always exists when $\omega_0 > \zeta(g) - 4JS(1 - \gamma_z)$. Evidently, if ω_0 is very close to $\zeta(g) - 4JS(1 - \gamma_z)$, then h_{cri} will also be close to zero, and its effect on the dynamics will not be so important, because the variation of the decay rate is quickly reversed by the increase of h.

The above condition explains the reason for which the critical features of the dynamics occur in the weak-coupling regime when $\gamma_z = 1$ (i.e., a Heisenberg lattice) practically for all values of ω_0, in contrast with the strong-coupling case. Indeed, even for small ω_0, there exists a value of h above which the decay rate always decreases, as was the case in the strong-coupling regime for large ω_0. Furthermore, for weak coupling, we notice the disappearance of the peak-shaped variation of the decay rate and the Lamb shift. This regime is best investigated through a perturbative treatment; the next section is devoted to these questions, which will be addressed in more detail when we derive the master equation within second-order perturbation theory.

Now we turn to the investigation of the evolution in time of the reduced density matrix of the impurity [see Fig. 5]. In accordance with the features exhibited by the decay rate, we find that, for small values of h, the matrix element ρ_{11}, which represents the occupation probability or population of the excited state, decreases faster as the value of h is raised and mostly tends asymptotically to values very close to zero. The variation is reversed as we cross the critical point h_{cri}, and the occupation probability decay becomes slower; in particular the asymptotic state assumes larger values at long times (see below for a quantitative discussion). For sufficiently strong magnetic field, the state of the impurity does not deviate much from its initial one. The time variation of the off-diagonal
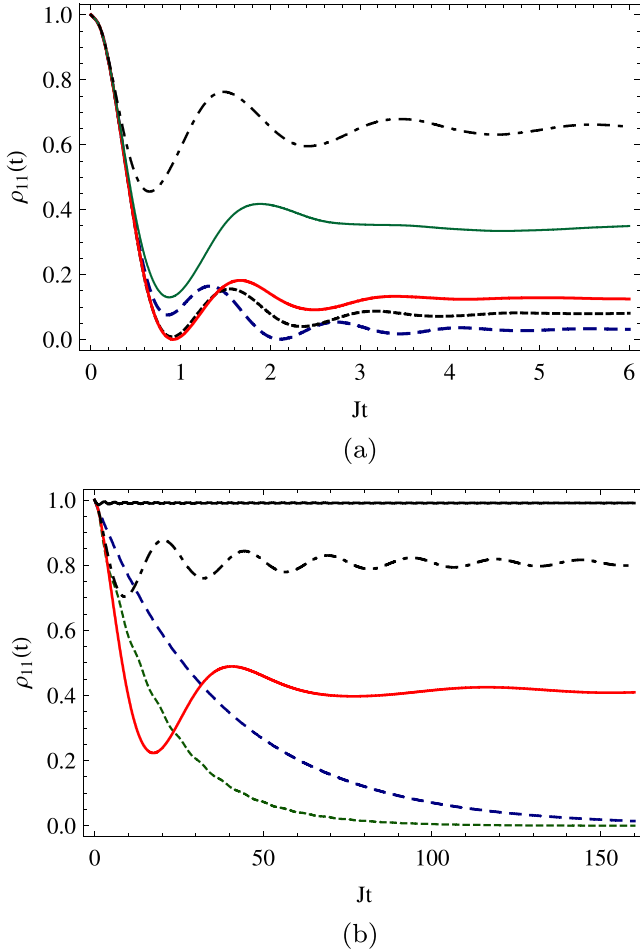
FIG. 5. The excited-state occupation probability as a function of time: (a) strong coupling with $h = 0.1J$ (blue dashed line), $h = J$ (black dotted line), $h = 1.5J$ (thick red solid line), $h = 3J$ (thin green solid line), and $h = 4J$ (blue dot-dashed line); other parameters are $\omega_0 = 3J$, $S = 1$, $g = J$, $\gamma_z = 1$. (b) Weak coupling with $h = 0.1J$ (blue dashed line), $h = 2J$ (green dotted line), $h = 3J$ (lower red solid line), $h = 3.2J$ (black dot-dashed line), and $h = 5J$ (upper black solid line); other parameters are $\omega_0 = 3J$, $g = 0.1J$, $S = 1$, $\gamma_z = 1$. The impurity initially occupies the exited state, i.e., $\rho_{11}(0) = 1$.

element ρ_{12} exhibits essentially the same characteristics. This implies that decoherence of the state of the impurity may be minimized at moderate times by applying a not too strong (weak) magnetic field, but the asymptotic state at long times will be nearly diagonal; on the contrary, if one is interested in the long-time behavior, it would be more convenient to apply a strong magnetic field.

The increase of the magnetic field should stabilize the ferromagnetic phase; this implies that, classically speaking, the lattice spins are more likely to be oriented along the z direction. The effective strength of the XY coupling should thus become weaker, leading to a lower decay rate. Our previous results, however, show that this is not the case at short to moderate intervals of time but holds only at longer times. Specifically, the loss of coherence of the impurity and the decay of the occupation probability become more significant as we approach h_{cri} from below.

The observed sharp decrease of the decay rate can be accounted for as the result of the fast revival of ρ_{11} when h is close to h_{cri}; the revival is produced after the occupation probability has completely vanished. This is explained by the back-flow of information from the lattice to the impurity due to memory effects; these features correspond to the non-Markovian character of the dynamics, which holds even in the weak-coupling regime. Specifically, we see from Fig. 5(b) that, for weak coupling, the near-exponential decay of the density-matrix element $\rho_{11}(t)$ is applicable only for small h; as we approach the critical point h_{cri}, the decay becomes mostly Gaussian, and the asymptotic probability does not vanish. A measure of the non-Markovianity of the dynamics may be realized by investigating the sign of the decay rate. In either regime, whether weak or strong, the revival of $\rho_{11}(t)$ corresponds to negative decay rates. Hence, we come to the important conclusion that, even in the weak-coupling regime, the dynamics displays strong non-Markovian behavior. It may be approximated by the exponential (Markovian) law in the weak-coupling regime only when the strength of the magnetic field is small enough, typically less than h_{cri} (see Sec. IV for more details).

Analytically, the asymptotic value of ϕ_+ can be determined by observing that by the Riemann-Lebesgue lemma,

$$\lim_{t\to\infty} \int_{\Omega_{\min}}^{\Omega_{\max}} \frac{\operatorname{Im} \Sigma_{\text{ret}}(\epsilon + i\nu)e^{-i\epsilon t}d\epsilon}{[\epsilon - \omega_0 - \operatorname{Re} \Sigma_{\text{ret}}(\epsilon + i\nu)]^2 + [\operatorname{Im} \Sigma_{\text{ret}}(\epsilon + i\nu)]^2}$$
$$= 0. \tag{34}$$

Therefore, we can distinguish between two cases: On the one hand, when the impurity possesses only one bound state, that is, when $\omega_0 \leqslant h + 4JS(1 + \gamma_z)h - g^2/J$, whose energy is ϵ_1, then

$$\lim_{t\to\infty} |\phi_+(t)|^2 = \frac{1}{\mathcal{B}(\epsilon_1)^2}, \tag{35}$$

$$\lim_{t\to\infty} \kappa(t) = 0, \tag{36}$$

where

$$\mathcal{B}(\epsilon) = 1 + \frac{4g^2}{[\epsilon - h - 4JS(1 - \gamma_z)]\big[\frac{J}{g^2}(\omega_0 - \epsilon) + 1\big]}. \tag{37}$$

The lamb shift $\xi(t)$ in turn tends to $2(\epsilon_1 - \omega_0)$. On the other hand, when the system exhibits two bound states, i.e., when $\omega_0 > h + 4JS(1 + \gamma_z)h - g^2/J$, whose energies are $\epsilon_1 < \epsilon_2$, then as $t \to \infty$:

$$|\phi_+(t)|^2 \sim \frac{1}{\mathcal{B}(\epsilon_1)\mathcal{B}(\epsilon_2)} \{\mathcal{D}(\epsilon_1, \epsilon_2) + 2\cos[(\epsilon_2 - \epsilon_1)t]\}, \tag{38}$$

$$\kappa(t) \sim \frac{2(\epsilon_2 - \epsilon_1)\sin[(\epsilon_2 - \epsilon_1)t]}{\mathcal{D}(\epsilon_1, \epsilon_2) + 2\cos[(\epsilon_2 - \epsilon_2)t]}, \tag{39}$$

where

$$\mathcal{D}(\epsilon_1, \epsilon_2) = \frac{\mathcal{B}(\epsilon_1)}{\mathcal{B}(\epsilon_2)} + \frac{\mathcal{B}(\epsilon_2)}{\mathcal{B}(\epsilon_1)}. \tag{40}$$

Hence, the asymptotic occupation probability oscillates in this case about $\mathcal{D}(\epsilon_1, \epsilon_2)/[\mathcal{B}(\epsilon_1)\mathcal{B}(\epsilon_2)]$. The decay rate also
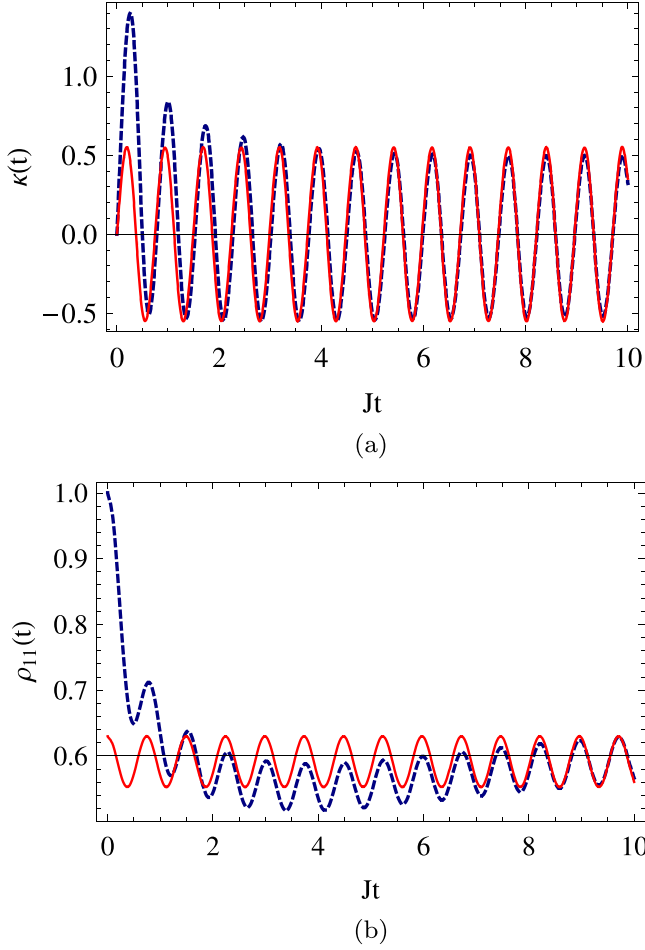
FIG. 6. Asymptotic behavior of (a) the decay rate κ, and (b) the excited-state population $\rho_{11}(t)$ in the case of two bound states: The red solid lines represent the asymptotic expressions of Eqs. (38) and (39), whereas the blue-dotted lines correspond to the exact solutions obtained by numerical integration of Eq. (29). The parameters are $g = J$, $h = 0.5J$, $\omega_0 = 8J$, $S = 1$, and $\gamma_z = 1$.

displays periodic oscillation with amplitude inversely proportional to $\mathcal{D}(\epsilon_1, \epsilon_2)$. This is illustrated in Fig. 6. Notice that the effect of the anisotropy parameter γ_z is merely to renormalize the magnetic field h in the low-excitation sector of the Hamiltonian. Indeed, all the discussion presented thus far could be interpreted in terms of the effective field $\tilde{h} = h + 2\eta J S \gamma_z$. This is equivalent to shifting the critical points by the value $2\eta J S \gamma_z$. Hence, from here on, we focus mainly on the variation of the magnetic field h and the impurity energy ω_0.

B. Two-dimensional lattice

We now consider the square lattice in two dimensions, for which the lattice constants in both the x and the y directions are the same and are equal to δ. Therefore, the first Brillouin zone corresponds to $-\pi/\delta \leqslant k_i \leqslant \pi/\delta$, $i \equiv x, y$. We further assume that the impurity lies in the center of a unit cell in the lattice so that the distance from it to any neighboring lattice spin is equal to $\delta/\sqrt{2}$. The coupling constant of the impurity to the lattice spins is denoted here also by g. Thus the squared modulus of the coupling constant $g_{\tilde{k}}$ is given by

$$|g_{\tilde{k}}|^2 = \frac{2Sg^2}{N}|1 + e^{ik_x\delta/2}(1 + e^{ik_y\delta/2} + e^{ik_x\delta/2})|^2$$

$$= \frac{32g^2S}{N}\cos^2(k_x\delta/2)\cos^2(k_y\delta/2). \tag{41}$$

Moreover, the lattice structure factor reads now as

$$\tau_{\tilde{k}} = \tfrac{1}{2}[\cos(k_x\delta) + \cos(k_y\delta)], \tag{42}$$

whereas the spectrum bounds are $\Omega_{\min} = \tilde{h} - 8JS$, and $\Omega_{\max} = \tilde{h} + 8JS$ (we use the notation $\tilde{h} = h + 8JS\gamma_z$). For a large number of sites, the lattice spectrum turns into a continuum of states; in this limit, the retarded self-energy may be expressed as

$$\Sigma_{\text{ret}}(\epsilon + i\nu) = \frac{8g^2S}{\pi^2}\int_{-\pi}^{\pi}\int_{-\pi}^{\pi}\frac{\cos^2(k_1/2)\cos^2(k_2/2)dk_1dk_2}{\epsilon - h - 8JS\gamma_z + 4JS[\cos(k_1) + \cos(k_2)] + i\nu}. \tag{43}$$

Outside the continuum, i.e., $\epsilon < \tilde{h} - 8JS$ or $\epsilon > \tilde{h} + 8JS$, the real part takes the form

$$\text{Re}\,\Sigma_{\text{ret}}(\epsilon + i0^+) = \frac{g^2}{2\pi SJ^2}\left[4\pi SJ - (\epsilon - \tilde{h})E\left(\frac{64S^2J^2}{(\epsilon - \tilde{h})^2}\right) + (\epsilon - \tilde{h} - 8JS)K\left(\frac{64S^2J^2}{(\epsilon - \tilde{h})^2}\right)\right], \tag{44}$$

where K and E are the complete elliptic integrals of the first and second kinds, respectively.

Inside the continuum, the integral in Eq. (43) cannot directly be performed. Thus we analytically continue the right-hand side of Eq. (44) by performing the analytic continuation of the complete elliptic integrals to the domain $|z| > 1$, $\text{Im}\,z < 0$ of the complex plane, namely [56]:

$$K(z) = \frac{1}{\sqrt{z}}\left[K\left(\frac{1}{z}\right) - iK\left(1 - \frac{1}{z}\right)\right], \tag{45}$$

$$E(z) = \sqrt{z}E\left(\frac{1}{z}\right) - \left(\frac{z-1}{\sqrt{z}}\right)K\left(\frac{1}{z}\right) + i\left[\sqrt{z}E\left(1 - \frac{1}{z}\right) - \frac{1}{\sqrt{z}}K\left(1 - \frac{1}{z}\right)\right]. \tag{46}$$
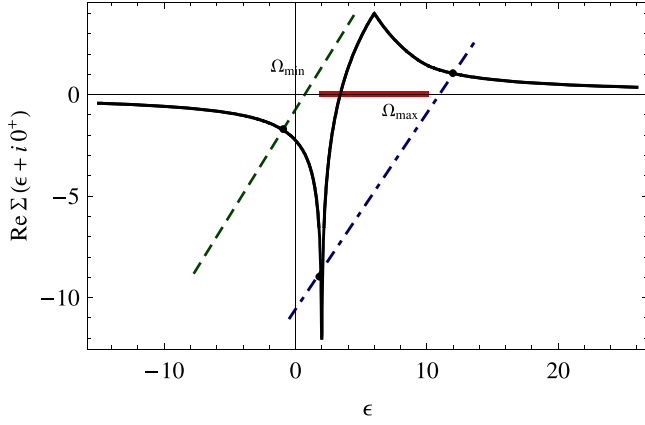
FIG. 7. The real part of the self-energy (black solid line) in a two-dimensional square lattice for $J = 0.5$, $g = 1$, $h = 2$, $S = 1$, and $\gamma_z = 1$. The intersection points correspond to the solutions of the equation $\mathrm{Re}\,\Sigma_{\mathrm{ret}}(\epsilon + i0^+) = \epsilon - \omega_0$ for $\omega_0 = 1$ (green dashed line) and $\omega_0 = 11$ (blue dot-dashed line); these solutions are interpreted in the main text as localized bound states outside the continuum.

This yields

$$
\begin{aligned}
&\mathrm{Re}\,\Sigma_{\mathrm{ret}}(\epsilon + i0^+) \\
&= \frac{2g^2}{J} - \frac{4g^2}{J\pi}\mathrm{sgn}(\epsilon - \tilde{h})E\!\left(\frac{(\epsilon - \tilde{h})^2}{64J^2S^2}\right) \\
&\quad + \frac{g^2}{2S\pi J^2}[8JS\,\mathrm{sgn}(\epsilon - \tilde{h}) - |\epsilon - \tilde{h}|]K\!\left(\frac{(\epsilon - \tilde{h})^2}{64J^2S^2}\right),
\end{aligned}
\tag{47}
$$

where $\mathrm{sgn}(x)$, denotes the sign of x.

Similarly, using the analytic continuation of $\Sigma(\epsilon)$, we find that, outside the continuum, $\mathrm{Im}\,\Sigma_{\mathrm{ret}}(\epsilon + i\nu) = 0$, whereas inside the continuum, the imaginary part is calculated as

$$
\begin{aligned}
\mathrm{Im}\,\Sigma_{\mathrm{ret}}(\epsilon + i0^+) &= \frac{g^2}{2\pi J}\left(\frac{\epsilon - \tilde{h}}{JS}\right)K\!\left(1 - \frac{(\epsilon - \tilde{h})^2}{64J^2S^2}\right) \\
&\quad - \frac{4g^2}{\pi J}E\!\left(1 - \frac{(\epsilon - \tilde{h})^2}{64J^2S^2}\right).
\end{aligned}
\tag{48}
$$

In this case, as depicted in Fig. 7, it turns out that the system exhibits two bound states when $\omega_0 > h + 8JS(1 + \gamma_z) - \mathrm{Re}\,\Sigma_{\mathrm{ret}}[h + 8JS(1 + \gamma_z) + i0^+]$. In the opposite situation, there exists only one localized bound state. Moreover, we see that, while in one dimension, the real part of the retarded self-energy of the impurity remains constant inside the continuum, in two dimensions, the same quantity diverges to negative values above and below the lower bound of the lattice spectrum; in particular, it increases as we approach the upper bound where it takes on a finite value. The knowledge of the explicit form of the real and imaginary parts of the retarded self-energy makes it possible to calculate the amplitude $\phi_+(t)$ and the decay rate $\kappa(t)$. The obtained results are depicted in Figs. 8–10 for both strong and weak coupling to the lattice. Here, again, it is found that the impurity dynamics is characterized by a critical dependence on the applied magnetic field; all the results we have presented earlier in the case of the one-dimensional lattice hold in the two-dimensional one. The main
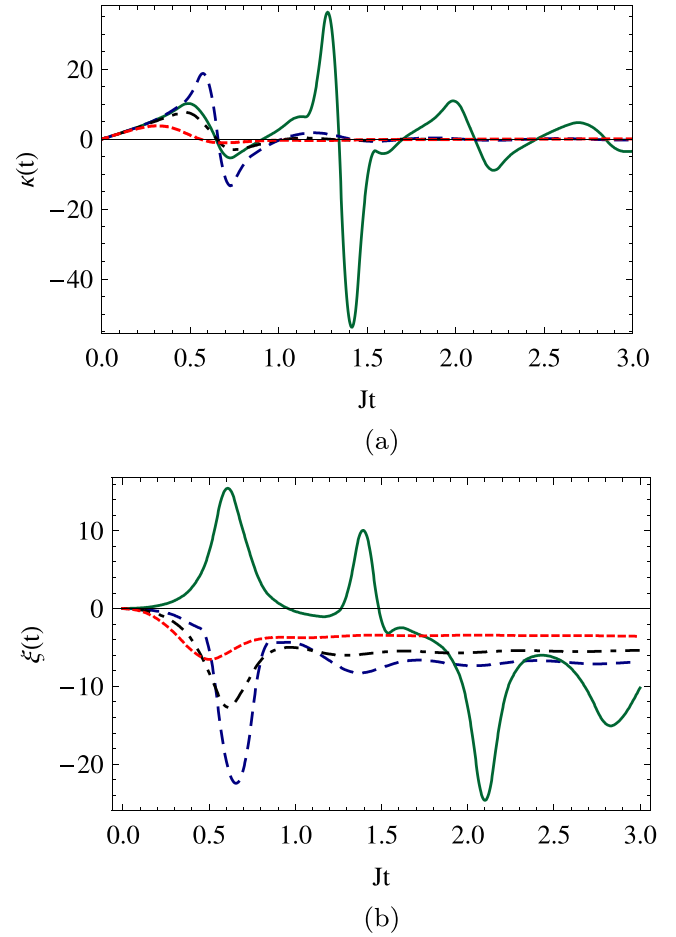

FIG. 8. (a) The decay rate κ, and (b) the Lamb shift ξ for strong coupling in two dimensions as a function of the time for different values of the strength of the magnetic field: $h = 0.1J$ (green solid lines), $h = 2J$ (blue dashed lines), $h = 3J$ (black dot-dashed lines), and $h = 5J$ (red dotted line); other parameters are $g = J$ $\omega_0 = 5J$, $S = 1$, $\gamma_z = 1$, $S = 1$.

difference rests in the order of magnitude of the quantities of interest, which basically is due to the increase of the number of nearest neighbors of the impurity. The asymptotic values of the excited-state occupation probability and the decay rate are given by expressions similar to Eqs. (35) and (36) for one bound state, and to equations (38) and (39) for two bound states but, in this case, we have

$$
\begin{aligned}
\mathcal{B}(\epsilon) &= 1 + \frac{g^2}{2\pi J^2 S}\left[\frac{\tilde{h} - \epsilon}{\tilde{h} - \epsilon - 8JS}E\!\left(\frac{(\epsilon - \tilde{h})^2}{64J^2S^2}\right)\right. \\
&\quad \left. - \frac{\tilde{h} - \epsilon + 8JS}{\tilde{h} - \epsilon}K\!\left(\frac{(\epsilon - \tilde{h})^2}{64J^2S^2}\right)\right].
\end{aligned}
\tag{49}
$$

It is interesting to notice that the features of the time evolution of the occupation probability, as obtained here, are quite similar to that of Refs. [25,27] in photonic crystals displaying band gaps, where the critical behavior depends on the detuning from the band edge. The effect of the latter is thus equivalent to the effect of the magnetic field in our spin system. While the oscillations in the photonic case for large detuning are due to reflections from the dielectric host, the
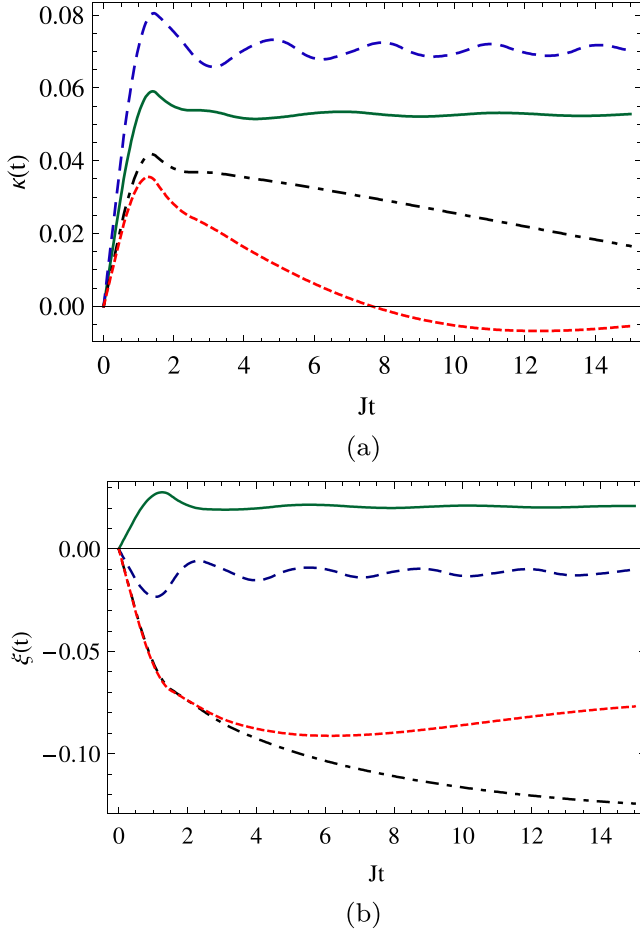
FIG. 9. (a) The decay rate, κ and (b) the Lamb shift ξ for weak coupling in two dimensions as a function of the time for different values of the strength of the magnetic field: $h = 0.1J$ (green solid lines), $h = 3J$ (blue dashed lines), $h = 5J$ (black dot-dashed lines), and $h = 5.2J$ (red dotted lines); other parameters are $g = 0.1J$, $\omega_0 = 5J$, $S = 1$, $\gamma_z = 1$, $S = 1$.
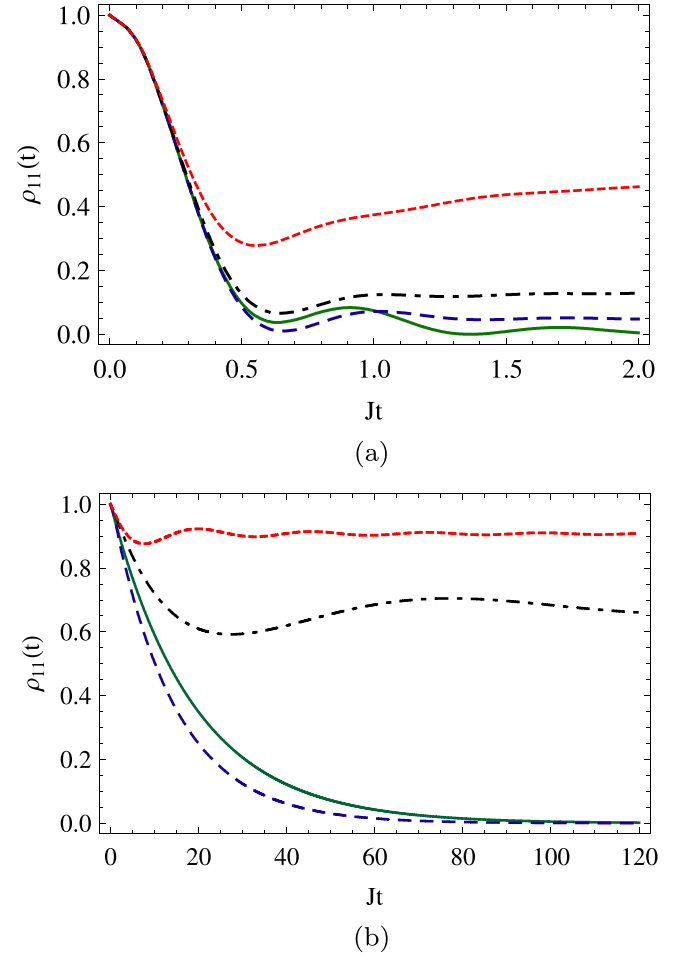

FIG. 10. The excited-state occupation probability as a function of the time in two dimensions. (a) Strong coupling with $h = 0.1J$ (green solid line), $h = 2J$ (blue dashed line), $h = 3J$ (black dot-dashed line), and $h = 5J$ (red dotted line); other parameters are $g = J$, $\omega_0 = 5J$, $S = 1$, and $\gamma_z = 1$. (b) Weak coupling with $h = 0.1J$ (green solid line), $h = 3J$ (blue dashed line), $h = 5J$ (black dot-dashed line), and $h = 5.2J$ (red doted line); other parameters are $g = 0.1J$, $\omega_0 = 5J$, $S = 1$, and $\gamma_z = 1$. The impurity initially occupies the excited state, i.e., $\rho_{11}(0) = 1$.

situation in the spin lattice has a different origin, namely, the inhibition of spin deviations in the lattice.

IV. WEAK-COUPLING REGIME: PERTURBATIVE TREATMENT

The present section is devoted to the investigation of the dynamics of the impurity in the weak-coupling regime. This means that the strength of the interaction is taken sufficiently weak so as to allow for a perturbative expansion with respect to the coupling constants g_k. For the sake of generality, we assume that the lattice is in thermal equilibrium at temperature T, and that its state is initially uncorrelated from that of the impurity. This makes it easier to derive the evolution equations, since the zero-temperature dynamics is simply obtained by letting $T \to 0$. A discussion of the nonzero-temperature case is given in the Appendix. This being said, it can now be shown that up to second order with respect to the coupling constants $g_{\bar{k}}$, the reduced density matrix verifies the master

equation:

$$
\frac{d\rho(t)}{dt} = -[(\omega_0 + \xi(t) - \xi^0(t)/2)\sigma_+\sigma_-, \rho(t)]
$$
$$
+ \kappa(t)\left(\sigma_-\rho(t)\sigma_+ - \frac{1}{2}\{\sigma_+\sigma_-, \rho(t)\}\right)
$$
$$
+ [\kappa(t) - \kappa^0(t)]\left(\sigma_+\rho\sigma_- - \frac{1}{2}\{\sigma_-\sigma_+, \rho\}\right), \quad (50)
$$

where $\kappa^0(t) = \kappa(t)|_{T=0}$, and $\xi^0(t) = \xi(t)|_{T=0}$. The decay rate and the Lamb shift at temperature T are given by

$$
\kappa(t) = 2\,\mathrm{Re}\,\Psi(t), \quad \xi(t) = 2\,\mathrm{Im}\,\Psi(t), \quad (51)
$$

with $\Psi(t)$ being the correlation function of the lattice, namely,

$$
\Psi(t) = \sum_k |g_{\bar{k}}|^2 e^{i(\omega_0 - \Omega_k)t}[n(\Omega_k) + 1]. \quad (52)
$$

In the above equation, $n(\Omega_k)$ denotes the mean number of magnons in mode k at temperature T, that is

$$n(\Omega_k) = \frac{1}{e^{\Omega_k/k_B T} - 1}. \tag{53}$$

At zero temperature, the master equation has the same form as the exact one (31), and the solution at $T = 0$ is thus given by (we drop the index)

$$\rho_{11}(t) = \rho_{11}(0) \exp\left\{ -\int_0^t \kappa(\tau)d\tau \right\}, \tag{54}$$

$$\rho_{12}(t) = \rho_{12}(0) \exp\left\{ -i\omega_0 t - \frac{i}{2}\int_0^t \xi(\tau)d\tau \right\}$$

$$\times \exp\left\{ -\frac{1}{2}\int_0^t \kappa(\tau)d\tau \right\}. \tag{55}$$

This form is quite general and is valid for both the exact and the second-order master equations. As a simple check, one can, for instance, insert $\kappa(t)$ as defined by Eq. (32) into Eq. (54) to end up with the impurity amplitude.

A. One-dimensional lattice

The correlation function in the continuum limit at zero temperature takes the form (after a change of variable):

$$\Psi(t) = 4Sg^2 e^{i(\omega_0 - h - 4JS\gamma_z)t} \int_{-1}^1 \frac{1+\zeta}{\pi\sqrt{1-\zeta^2}} e^{i4JSt\zeta}d\zeta. \tag{56}$$

This integral can be evaluated exactly by using the Bessel functions of the first kind, denoted here by $\mathbf{J}_n$, yielding

$$\Psi(t) = 4Sg^2 e^{i(\omega_0 - h - 4JS\gamma_z)t} [\mathbf{J}_0(4JSt) + i\mathbf{J}_1(4JSt)]. \tag{57}$$

Consequently, the decay rate κ can be expressed as [see Eq. (51)]

$$\kappa(t) = 8g^2 S \int_0^t dt' \{\cos[(\omega_0 - \tilde{h})t']\mathbf{J}_0(4JSt')$$
$$- \sin[(\omega_0 - \tilde{h})t']\mathbf{J}_1(4JSt')\}, \tag{58}$$

whereas the Lamb-shift ξ takes the form

$$\xi(t) = 8g^2 S \int_0^t dt' \{\sin[(\omega_0 - \tilde{h})t']\mathbf{J}_0(4JSt')$$
$$+ \cos[(\omega_0 - \tilde{h})t']\mathbf{J}_1(4JSt')\}. \tag{59}$$

In Fig. 11, we compare the decay rate and the matrix element ρ_{11} obtained here with the exact ones of Sec. III. It can be seen that the agreement is excellent for relatively long periods of time. In general, however, the two solutions do not coincide asymptotically, which is to be expected. In fact, the long-time behavior in this second-order approximation overestimates the actual exact values of the decay rate and the Lamb shift. Let us investigate the asymptotic values of the latter quantities in the present approximation, which turn out to be given by $\kappa_{\text{mark}} = \lim_{t\to\infty} \kappa(t) = 0$ for $4JS < |\omega_0 - h - 4JS\gamma_z|$, whereas

$$\kappa_{\text{mark}} = \frac{2g^2}{J}\sqrt{\frac{4JS - \omega_0 + h + 4JS\gamma_z}{\omega_0 - h - 4JS\gamma_z + 4JS}} \tag{60}$$
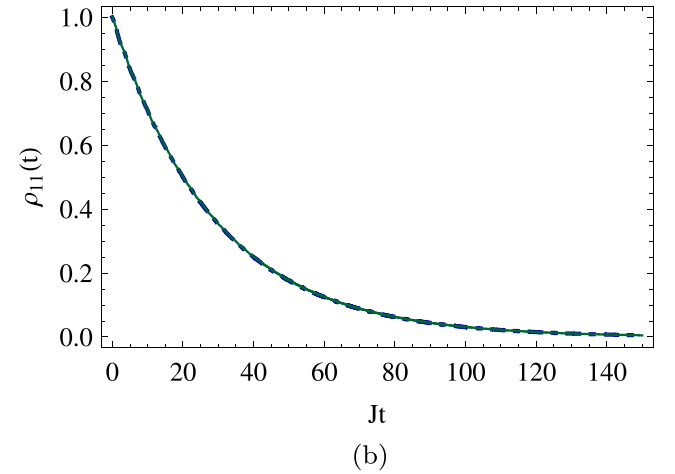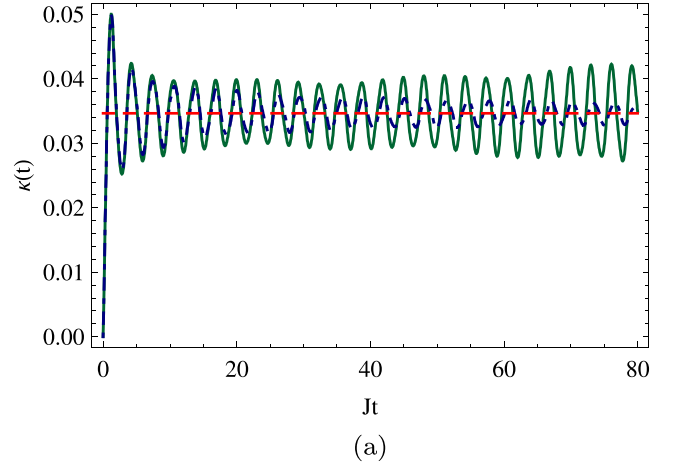
(a)

(b)

FIG. 11. Comparison between the exact numerical solutions in one dimension (green solid lines) and the outcomes of the second-order master equation (blue dot-dashed lines) in the weak-coupling regime for (a) the decay rate and (b) the excited-state occupation probability; the parameters are $g = 0.1J$, $h = J$, $\omega_0 = 3J$, $S = 1$, $\gamma_z = 1$, and $\rho_{11}(0) = 1$. The horizontal red dashed line represents the Markovian decay rate. Notice that the two solutions for the occupation probability are almost identical for the chosen value of h.

for $4JS > |\omega_0 - h - 4JS\gamma_z|$. Similarly, we find that $\xi_{\text{mark}} = \lim_{t\to\infty} \xi(t) = \frac{2g^2}{J}$ for $4JS > |\omega_0 - h - 4JS\gamma_z|$ and

$$\xi_{\text{mark}} = \frac{2g^2}{J}\left(1 - \frac{|\omega_0 - h - 4JS(1+\gamma_z)|}{\sqrt{(\omega_0 - h - 4JS\gamma_z)^2 - (4JS)^2}}\right) \tag{61}$$

for $4JS < |\omega_0 - h - 4JS\gamma_z|$, which are exactly the values of the decay rate and the Lamb shift obtained in the Markov approximation. The latter results are actually a manifestation of the breakdown of the Fermi golden rule, which states, for instance, that, for weak coupling, the decay rate and the Lamb shift are given by $\kappa_{\text{mark}} = 2\,\text{Im}\,\Sigma_{\text{ret}}(\omega_0 + i0^+)$, and $\xi_{\text{mark}} = 2\,\text{Re}\,\Sigma_{\text{ret}}(\omega_0 + i0^+)$.

We have already noticed in Sec. III that, in the weak-coupling regime, the Markovian decay law $e^{-\kappa_{\text{mark}}t}$ is valid only for weak magnetic field. The reason behind this resides in the fact that the decay of the correlation function of the lattice is fast enough only when h is small. The larger the values of

h, the slower the decay of the correlation function is; the latter exhibits in particular oscillatory variation at long times, and hence the dynamics deviates from the exponential law to the Gaussian one; in all cases, the long-time limit of the quantities κ and ξ exists thanks to the properties of the Bessel functions of the first kind. The decay of the correlation function is a general property of the weak coupling to continua, which is the case in this model. The breakdown of the Fermi golden rule is best illustrated by the vanishing value of the decay rate $\kappa_{\text{mark}} = 0$ for $4JS < |\omega_0 - h - 4JS\gamma_z|$. Hence, if we apply directly the latter rule, we find that there occurs no decay of the state of the impurity; in other words, the impurity does not feel at all the presence of the lattice despite its coupling to the latter, which is not necessarily the case as is confirmed by the exact solution of the previous section. It is also worthwhile noticing that, although the Markovian limit fails to reproduce the actual dynamics at long times, it keeps track of the overall critical behavior of the impurity, as is discussed below.

Resonance-like behavior

A particular instance occurs when ω_0 coincides with Ω_k in the center or at the edges of the first Brillouin zone, that is, for $k = 0, \pm\pi$. In this resonance-like case, we can distinguish two possible situations, namely $\omega_0 - h - 4JS\gamma_z = \pm 4JS$. We begin with the condition $\omega_0 = h + 4JS(\gamma_z - 1)$, which should be compared with the one obtained in Sec. III for h_{cri}, evaluated in the weak-coupling regime $g \ll J$, i.e., $h_{\text{cri}} = 4JS(1 - \gamma_z) + \omega_0$. The latter relation is a very peculiar condition that links the energy of the two-level impurity to the lower limit of the spectrum of the lattice. It occurs precisely in the center of the first Brillouin zone. The particular feature of the decay rate and the Lamb shift in this case rests in the fact that they grow relatively fast as time increases; in particular, we find that the Markovian limits diverge since $\lim_{t\to\infty} \kappa(t) = \lim_{t\to\infty} |\xi(t)| = \infty$. A comparison between the exact decay rate and the perturbative one is carried out in Fig. 12, where we can see that, initially, the two coincide at short times, but eventually the exact decay rate tends asymptotically to zero. We also notice that, while the approximate decay rate remains positive, the exact one takes negative values, indicating regeneration of both the excited-state occupation probability and the quantum interferences (recoherence). On the other hand, when $\omega_0 = h + 4JS(1 + \gamma_z)$ we obtain a rather reduced decay rate and, in particular, it turns out that $\kappa(t) \to 0$ while $\xi(t) \to 2g^2/J$ as $t \to \infty$; this indicates that there occurs no divergence of the decay rate and the Lamb shift in the Markov approximation.

It should be noted that the condition $4JS \leqslant |\omega_0 - h - 4JS\gamma_z|$ is equivalent to the statement that ω_0, the characteristic intrinsic energy-level spacing of the impurity, lies within the continuum associated with the lattice. The divergence of the Markovian decay rate may typically be attributed to a resonance in the center of the first Brillouin zone where $\omega_0 = h + 4JS(\gamma_z - 1)$. This can be explained by the coupling of the impurity to the collective mode zero of the spin degrees of freedom of the lattice. In this mode, the effects of the quantum excitations or magnons add to each other coherently, and hence it dominates over the other modes. Indeed, by
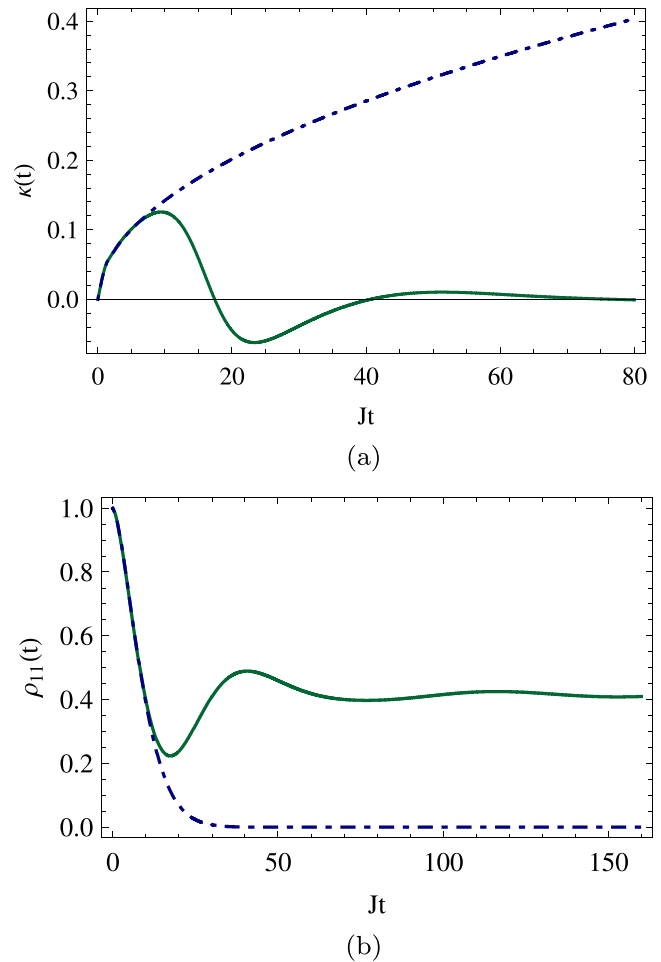
(a)

(b)

FIG. 12. The same as Fig. 11 but for $h = \omega_0 = 3J$ (resonance).

inspecting Eq. (56), we see that the spectral function is given by $f(z) = (1 + z)/\pi(1 - z^2)^{1/2}$, which clearly displays a Van Hove singularity only in the center of the first Brillouin zone, i.e., when $z = 1$ or equivalently $k = 0$, and vanishes at its edges where $z = -1$, which corresponds to $k = \pm\pi$. Once the parameter ω_0 exceeds the lower bound, the decay rate begins to decrease as the former approaches the upper bound of the spectrum. The above variation persists even when ω_0 exits the continuum. When $\omega_0 < h$, the resonance condition cannot be satisfied, which explains the absence of the critical divergence in the Markov limit.

B. Two- and three-dimensional lattices

The decay of the correlation function in two and three-dimensional lattices is much faster than that of the one-dimensional lattice even for small h; the suppression of the oscillations is more noticeable at shorter times. The exact decay rate and the excited-state occupation probability ρ_{11}, along with the approximate ones, are illustrated in Fig. 13 for $d = 2$. The agreement is good for long times. Furthermore, applying the Fermi golden rule, the Markovian decay rate in the case of the square lattice vanishes for $|\omega_0 - \tilde{h}| > 8JS$;
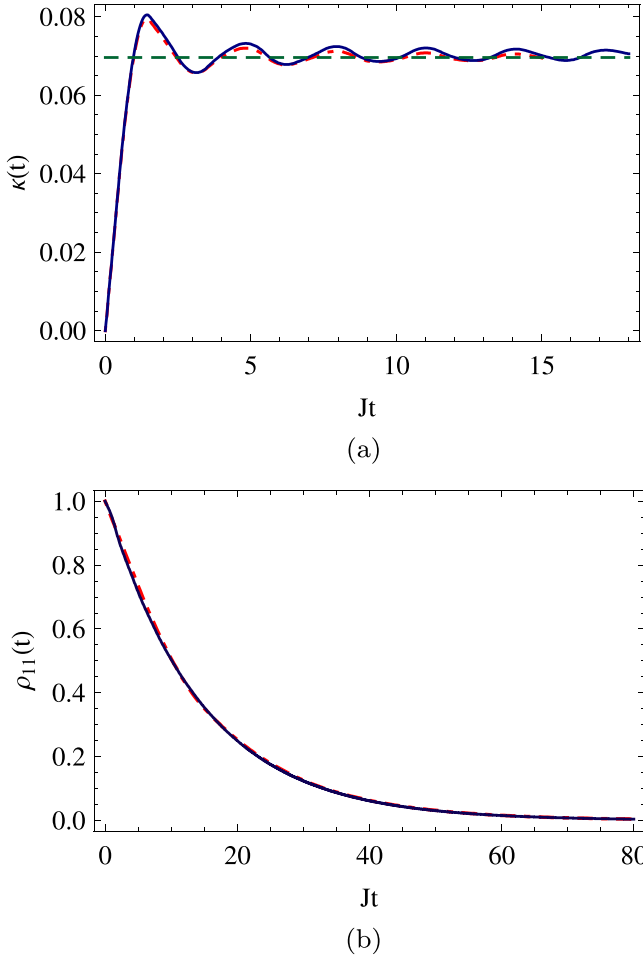
(a)

(b)

FIG. 13. Time evolution of (a) the decay rate κ and (b) the excited-state occupation probability ρ_{11} in two dimensions at resonance with $h = \omega_0 = 5J$ for weak coupling of the impurity: exact solution (blue solid lines), and the solution of the second-order master equation (red dot-dashed lines). The other parameters are $g = 0.1J$, $S = 1$, and $\gamma_z = 1$. Notice the complete suppression of oscillations at long times in two dimensions.

when $|\omega_0 - \tilde{h}| < 8JS$ it is given by

$$\kappa_{\text{mark}} = -\frac{g^2}{\pi J}\left(\frac{\omega_0 - \tilde{h}}{JS}\right)K\left(1 - \frac{(\omega_0 - \tilde{h})^2}{64J^2S^2}\right)$$
$$+ \frac{8g^2}{\pi J}E\left(1 - \frac{(\omega_0 - \tilde{h})^2}{64J^2S^2}\right). \quad (62)$$

At resonance, $h - \omega_0 = 8JS(1 - \gamma_z)$, the Markovian decay rate remains finite; indeed, on account of the fact that $K(0) = E(0) = \frac{\pi}{2}$, it follows that

$$\kappa_{\text{mark}} = \frac{4g^2}{J}. \quad (63)$$

If the impurity possesses one bound state, the exact decay rate vanishes at infinity, and hence it differs significantly from the Markovian rate, see Fig. 14.

The coupling constant in a three-dimensional simple cubic lattice, where the impurity occupies the center of a unit cell,
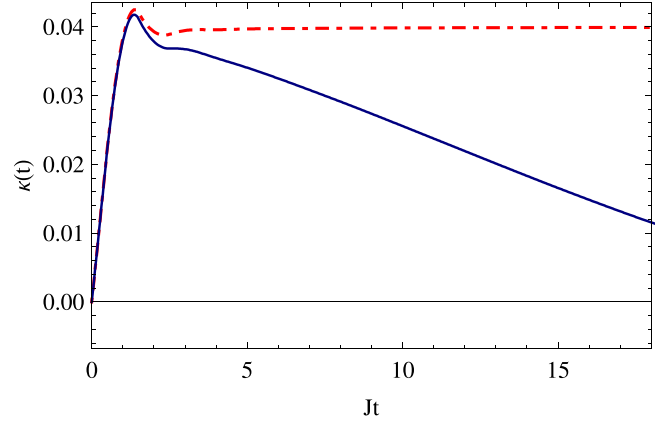

FIG. 14. The decay rate in two dimensions as a function of time: exact solution (blue solid line), and the second-order approximation (red dot-dashed line). The parameters are $h = 3J$, $\omega_0 = 5J$, $g = 0.1J$, $S = 1$, and $\gamma = 1$.

is given by

$$g_{\vec{k}} = g\sqrt{\frac{2S}{N}}\left\{\cos\left[\frac{\delta}{2}(k_x + k_y + k_z)\right] + \cos\left[\frac{\delta}{2}(k_x - k_y + k_z)\right]\right.$$
$$\left. + \cos\left[\frac{\delta}{2}(k_x + k_y - k_z)\right] + \cos\left[\frac{\delta}{2}(-k_x + k_y + k_z)\right]\right\}. \quad (64)$$

It follows that

$$|g_{\vec{k}}|^2 = \frac{128g^2S}{N}\cos(\delta k_x/2)^2 \cos(\delta k_y/2)^2 \cos(\delta k_z/2)^2. \quad (65)$$

The integration with respect to the wave vector $\vec{k}$ in the continuum limit is more involved here, but we can nevertheless draw the following conclusion: The density of states of the lattice is finite; therefore, the decay rate and the Lamb shift in the Markovian limit do not diverge, even at resonance, as illustrated in Fig. 15. Here, also, the time evolution depends on whether h exceeds the critical value, which turns out to be $h_{\text{cri}} = \omega_0 + 12JS(1 - \gamma_z)$.
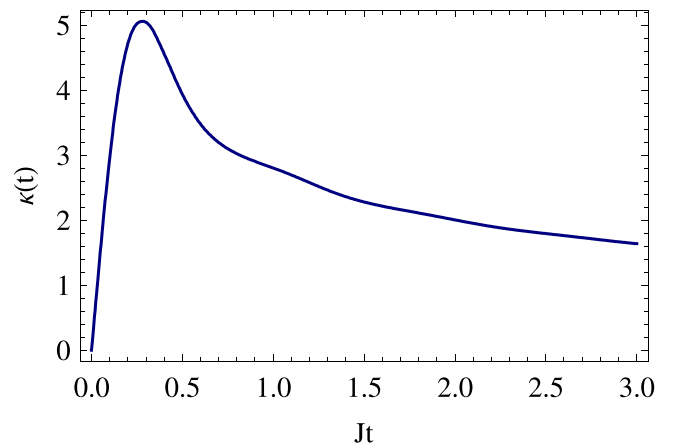

FIG. 15. The approximate decay rate in three dimensions at resonance with $h = \omega_0 = 3J$ for weak coupling of the impurity. The other parameters are $g = 0.1J$, $S = 1$, and $\gamma_z = 1$.
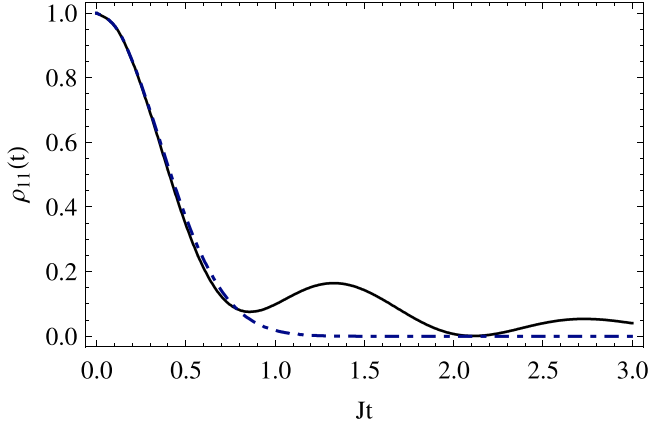
FIG. 16. Comparison between the exact numerical solution in one dimension (black solid line) and the short-time approximation (blue dot-dashed line) of Eq. (69). The parameters are $g = J$, $h = 0.1J$, $\omega_0 = 3J$, $S = 1$, $\gamma_z = 1$, and $\rho_{11}(0) = 1$.

C. Short-time variation

From the above discussion, one can conclude that, in a d-dimensional lattice, we have in general

$$|g_{\bar{k}}|^2 = \frac{2^{2d+1}g^2 S}{N} \prod_{i=x,y,z} \cos(\delta k_i/2)^2. \tag{66}$$

By expanding the integrand of Eq. (58) in a Taylor series and integrating term by term, it follows that, in the continuum limit, the variation of the decay rate at short times is described by

$$\kappa(t) = 2^{d+2}g^2 S t + O(t^3), \tag{67}$$

which is linear in time and is independent of the magnetic field. This, however, is not the case for the Lamb shift, which is affected by both the magnetic field and the impurity energy. For instance, in $d = 1$, it turns out that

$$\xi(t) = 4g^2 S[\omega_0 - h + 2JS(1 - 2\gamma_z)]t^2 + O(t^4). \tag{68}$$

Therefore, if $h + 4JS(\gamma_z - 1/2) > \omega_0$, the coefficient of t^2 becomes negative, in complete accordance with the observed decrease of the Lamb shift to negative values.

Taking into account Eqs. (54) and (55), we obtain that, at short times,

$$\rho_{11}(t) \simeq \rho_{11}(0)e^{-2t^2/\tau_D^2}, \tag{69}$$

$$|\rho_{12}(t)| \simeq |\rho_{12}(0)|e^{-t^2/\tau_D^2}, \tag{70}$$

where the decoherence time constant τ_D is defined by

$$\tau_D = \frac{1}{2^{d/2}g\sqrt{S}}. \tag{71}$$

These expressions are best applied to the strong-coupling regime; they turn out to be a very good approximation in particular for small values of h, as illustrated in Fig. 16, where we display the exact evolution in time of the density-matrix element $\rho_{11}(t)$ along with the approximate one given by Eq. (69).

The linear dependence of the decay rate, together with the quadratic behavior of the decay of the reduced density matrix
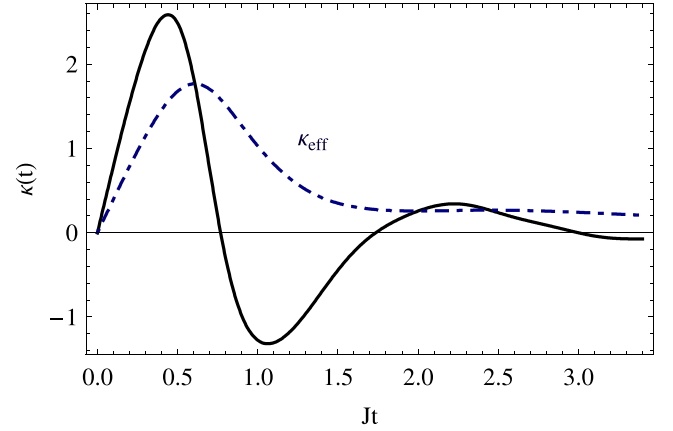

FIG. 17. The exact (black solid line) and the effective (blue dot-dashed line) decay rates in one dimension as a function of time for $g = J$, $h = 3J$, $\omega_0 = 2J$, $S = 1$, and $\gamma_z = 1$.

at short times are known to correspond to the so-called Zeno regime [57–70]. The investigation of this regime in the context of the present work makes the subject of the next section.

V. APPLICATION TO THE QUANTUM ZENO EFFECT

Let us begin by recalling the main ideas behind the concept of the quantum Zeno effect (QZE) as applied to the impurity [68]. Suppose that the latter is initially prepared in the excited state, which is equivalent to setting $\rho_{11}(0) = 1$. As the time evolves, the so-called survival probability is given by $P(t) = \rho_{11}(t)$. This is the probability of finding the impurity at later times in the initial state. If a series of N measurements are performed at regular time intervals τ, the survival probability becomes

$$P(N\tau) = P(\tau)^N = \rho_{11}(\tau)^N. \tag{72}$$

An effective decay rate is introduced via the identity

$$P(N\tau) = e^{-\kappa_{\text{eff}}(\tau)t}, \tag{73}$$

where $t = N\tau$. Notice that, by Eq. (30), we have $\rho_{11}(t) = |\phi_+(t)|^2$; it immediately follows that

$$\kappa_{\text{eff}}(\tau) = -\frac{1}{\tau}\ln[\rho_{11}(\tau)] = -\frac{1}{\tau}\ln|\phi_+(\tau)|^2, \tag{74}$$

which should be compared with the exact decay rate of Eq. (32) that can be written as

$$\kappa(t) = -\frac{d\ln|\phi_+(t)|^2}{dt}. \tag{75}$$

The two decay rates are generally different, as illustrated in Fig. 17. In fact, even at short times, the above expressions yield distinct outcomes. For instance, consider the weak-coupling regime, which is described by Eqs. (52) and (54) at $T = 0$. These give

$$\int_0^t \kappa(t')dt' = 2\sum_k |g_k|^2 \int_0^t \frac{\sin[(\omega_0 - \Omega_k)t']}{\omega_0 - \Omega_k}dt'$$

$$= 2t^2 \sum_k |g_k|^2 \frac{\sin^2[(\omega_0 - \Omega_k)t/2]}{[(\omega_0 - \Omega_k)t/2]^2}. \tag{76}$$

Therefore, for a measurement time τ:

$$\int_0^\tau \kappa(t')dt' = 2\tau\kappa_{\mathrm{eff}}(\tau), \qquad (77)$$

where [68–70]

$$\kappa_{\mathrm{eff}}(\tau) = \tau \sum_k |g_k|^2 \frac{\sin^2[(\omega_0 - \Omega_k)\tau/2]}{[(\omega_0 - \Omega_k)\tau/2]^2}. \qquad (78)$$

For small measurement time, we have:

$$\int_0^\tau \kappa(t')dt' \simeq [\kappa(\tau) - \kappa(0)]\tau = \tau\kappa(\tau), \qquad (79)$$

which shows that the effective decay rate is twice smaller than the exact decay rate. In fact if we keep only terms linear in τ in the expansion of the sine function, we end up with

$$\kappa_{\mathrm{eff}}(\tau) = 2^{d+1}g^2 S\tau = \frac{\kappa(\tau)}{2}, \qquad (80)$$

in complete agreement with Eq. (67) describing the short-time variation at zero temperature. Notice, moreover, that the effective decay rate remains always positive at all times, which is obvious from its definition because $|\phi_+(\tau)|^2 \leqslant 1$. This means that, for large τ, the effective decay rate is insensitive to the regions of negative exact decay rate, which correspond to recoherence effects, as we have mentioned earlier. From the above results, we see that one obtains always the QZE at short times, as the measurement slows the decay of the impurity. At larger times, however, one may thus obtain the quantum inverse Zeno effect (IZE) [70]. The recoherence effects become more appreciable for large values of magnetic field; for such values, the measurement may have a destructive effect on the coherences of the impurity, and may thus also lead to the acceleration of the decay of the survival probability.

More importantly, it becomes clear from Eq. (80) that, if the measurement is performed at timescales for which the latter equation is valid, the impurity evolution becomes independent of both the magnetic field h and the intrinsic level energy spacing ω_0. In particular, when $h > h_{\mathrm{cri}}$ the measurement speeds up the decay of the survival probability, preventing thus the magnetic field from protecting the impurity state from the effect of the lattice, which is a direct consequence of the IZE.

Let us now assume that h is small enough so that we ascertain that the Fermi golden rule holds for weak coupling. Under these conditions, the Markovian decay rate defines the natural lifetime $1/\kappa_{\mathrm{mark}}$ of the impurity. In this case, according to Ref. [68], the criterion for the QZE to happen is that τ be smaller than τ^*, the solution of the equation $\kappa_{\mathrm{eff}}(\tau^*) = \kappa_{\mathrm{mark}}$. When $\tau > \tau^*$, the IZE takes place. We have seen that, for $\omega_0 < h - 2J\eta S(1 - \gamma_z)$ or $\omega_0 > h + 2J\eta S(1 + \gamma_z)$, the Markovian decay rate vanishes, i.e., $\kappa_{\mathrm{mark}} = 0$. In this case there exists no solution for the latter equation, and we obtain always the IZE.

VI. CONCLUSION

The present study gives a thorough discussion of the dynamics of a two-level impurity that is coupled through an

XY interaction to a ferromagnetic lattice at low temperatures. Under the condition of small lattice excitations, our model is equivalent to the Fano-Anderson one, with a particular form of the coupling constant, which is due to the geometric configuration of the system where the impurity occupies the center of a unit cell in the lattice. This makes it possible to derive in an exact manner the zero-temperature retarded Green's function in one and two dimensions. The latter is directly linked to the excited-state amplitude, which is found to satisfy a master equation in Lindblad form involving the decay rate and the Lamb shift. By studying the evolution of those quantities, we find that, under certain conditions, there exists a critical value of the magnetic field above which the decay always slows down. In the weak-coupling regime, the critical point occurs when the impurity energy coincides with the lower bound of the continuum. In particular, in the case of the Heisenberg model, for which the anisotropy parameter γ_z is set to unity, the critical magnetic field is identical to the impurity level energy spacing, which we termed resonance. The investigation reveals that in this regime, the Fermi golden rule does
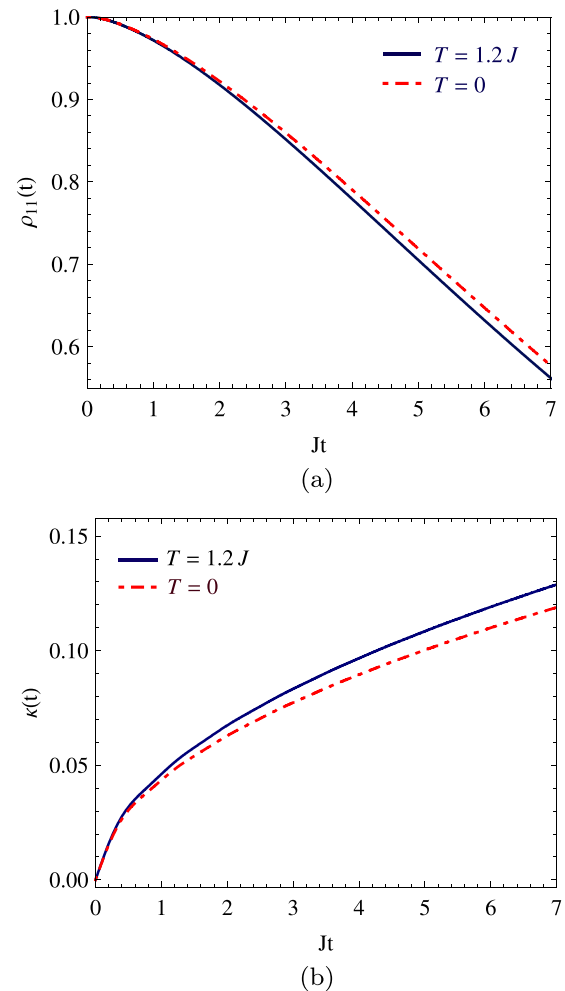

FIG. 18. The time dependence of (a) the excited-state population ρ_{11}, and (b) the decay rate κ at zero temperature (red dot-dashed lines) and nonzero temperature (blue solid lines) in the weak-coupling regime at resonance with $g = 0.1J$, $h = \omega_0 = 3J$, $S = 1$, $\gamma_z = 1$, and $\rho_{11}(0) = 1$ (we set $k_B = 1$).

not apply if the magnetic field exceeds the critical value. The exponential decay law holds only for weak magnetic fields, for which the lattice correlation function is damped fast enough so that the conditions of the Markovian approximation are fulfilled. We have derived the master equation for the reduced density matrix of the purity in the weak-coupling regime. The elimination of the lattice degrees of freedom is carried out by taking into account the spectral properties of the lattice which are uniquely fixed by its dispersion relation. The validity of the master equation is discussed by comparing its outcome with the exact solution. At resonance, the Markovian decay rate and the Lamb shift diverge in one dimension but remain finite at higher dimensions. The effective decay rate of the Zeno effect is found to be insensitive to regions of negative decay rate, and hence the measurement may lead to the inverse Zeno effect, as the decay may be accelerated, in particular for strong magnetic field.

ACKNOWLEDGMENTS

The author would like to thank the referee for the valuable suggestions and comments.

APPENDIX: EFFECT OF THE TEMPERATURE

The spin-wave formalism is applicable at low temperatures, where the number of magnons or excitations is small. The main criterion for the use of the Holstein-Primakoff transformation is $n(\Omega_k) \ll 2S$ for all modes. Actually, it is sufficient that the lower bound of the lattice spectrum $\Omega_{\min} = h + 2JS\eta(\gamma_z - 1)$ verifies the above criterion to ensure that the mean numbers of magnons in all modes are small enough, which can be formulated as

$$\left(e^{[h+2SJ\eta(\gamma_z-1)]/k_BT} - 1\right)^{-1} \ll 2S. \tag{A1}$$

For temperatures satisfying the latter condition, the density matrix in the weak-coupling regime is described by the master equation (50). It is a matter of algebra to show that its solution

is given by

$$\rho_{11}(t) = \exp\left\{-\int_0^t [2\kappa(\tau) - \kappa^0(\tau)]d\tau\right\}$$
$$\times \left[\rho_{11}(0) + \int_0^t [\kappa(\tau) - \kappa^0(\tau)] \exp\left\{\int_0^\tau [2\kappa(\tau')\right.\right.$$
$$\left.\left.- \kappa^0(\tau')]d\tau'\right\}d\tau\right], \tag{A2}$$

$$\rho_{12}(t) = \rho_{12}(0)\exp\left\{-i\omega_0 t - \frac{i}{2}\int_0^t [2\xi(\tau) - \xi^0(\tau)]d\tau\right\}$$
$$\times \exp\left\{-\frac{1}{2}\int_0^t [2\kappa(\tau) - \kappa^0(\tau)]d\tau\right\}. \tag{A3}$$

Figure 18 gives an example of the time variation of the decay rate at nonzero temperature in one dimension. It can be seen that, as expected, the decay rate becomes larger as the temperature raises, which is due to the fact that the number of magnons becomes more important, leading to greater deviations of the spin vectors toward the x-y plane; as a result, the effective XY coupling of the impurity to the lattice also grows. At such low temperatures, the critical dependence of the decay rate on the magnetic field still holds, which means that the Markovian decay rate diverges when $h = \omega_0 + 4JS(1 - \gamma_z)$.

At sufficiently short times, we may approximate the reduced density matrix elements by

$$\rho_{11}(t) = e^{-2\Gamma t^2}\left(\rho_{11}(0) - \frac{\Delta}{\Gamma}\right) + \frac{\Delta}{\Gamma}, \tag{A4}$$

$$|\rho_{12}(t)| = |\rho_{12}(0)|e^{-\Gamma t^2}, \tag{A5}$$

where

$$\Gamma = \frac{1}{2}\sum_k |g_k|^2 [2n(\Omega_k) + 1], \tag{A6}$$

$$\Delta = \frac{1}{2}\sum_k |g_k|^2 n(\Omega_k). \tag{A7}$$

It follows that the temperature-dependent decoherence time constant is given by

$$\tau_D = \frac{\sqrt{2}}{\sqrt{\sum_k |g_k|^2 [2n(\Omega_k) + 1]}}. \tag{A8}$$

[1] H.-P. Breuer and F. Petruccione, *The Theory of Open Quantum Systems* (Oxford University Press, Oxford, 2002).

[2] W. H. Zurek, Phys. Today **44**, 36 (1991).

[3] D. P. DiVincenzo and D. Loss, J. Magn. Magn. Mater. **200**, 202 (1999).

[4] W. H. Zurek, Rev. Mod. Phys. **75**, 715 (2003).

[5] E. T. Jaynes and F. W. Cummings, Proc. IEEE **51**, 89 (1963).

[6] A. V. Khaetskii, D. Loss, and L. Glazman, Phys. Rev. Lett. **88**, 186802 (2002).

[7] W. A. Coish and D. Loss, Phys. Rev. B **70**, 195340 (2004).

[8] W. Zhang, V. V. Dobrovitski, K. A. Al-Hassanieh, E. Dagotto, and B. N. Harmon, Phys. Rev. B **74**, 205313 (2006).

[9] L. Amico, R. Fazio, A. Osterloh, and V. Vedral, Rev. Mod. Phys. **80**, 517 (2008).

[10] X.-Z. Yuan, H.-S. Goan, and K.-D. Zhu, Phys. Rev. B **75**, 045331 (2007).

[11] Z. Huang and G. Sadiek, and S. Kais, J. Chem. Phys. **124**, 144513 (2006).

[12] B. Alkurtass, G. Sadiek, and S. Kais, Phys. Rev. A **84**, 022314 (2011).

[13] H.-P. Breuer, D. Burgarth, and F. Petruccione, Phys. Rev. B **70**, 045323 (2004).

[14] Y. Hamdouni, M. Fannes, and F. Petruccione, Phys. Rev. B **73**, 245323 (2006).

[15] Y. Hamdouni and F. Petruccione, Phys. Rev. B **76**, 174306 (2007).

[16] Y. Hamdouni, J. Phys. A: Math. Theor. **40**, 11569 (2007); **42**, 315301 (2009); Phys. Lett. A **373**, 1233 (2009); J. Phys. A: Math. Theo. **45**, 425301 (2012).

[17] M. Lucamarini, S. Paganelli, and S. Mancini, Phys. Rev. A **69**, 062308 (2004).

[18] W. T. Strunz, L. Diósi, and N. Gisin, Phys. Rev. Lett. **82**, 1801 (1999).

[19] J. Piilo, S. Maniscalco, K. Härkönen, and K.-A. Suominen, Phys. Rev. Lett. **100**, 180402 (2008).

[20] J. Piilo, K. Härkönen, S. Maniscalco, and K.-A. Suominen, Phys. Rev. A **79**, 062112 (2009).

[21] U. Fano, Phys. Rev. **124**, 1866 (1961).

[22] P. W. Anderson, Phys. Rev. **124**, 41 (1961).

[23] G. D. Mahan, *Many-Particle Physics*, 2nd ed. (Plenum Press, New York, 1990).

[24] A. J. Leggett, S. Chakravarty, A. T. Dorsey, M. P. A. Fisher, A. Garg, and W. Zwerger, Rev. Mod. Phys. **59**, 1 (1987).

[25] S. John and T. Quang, Phys. Rev. A **50**, 1764 (1994).

[26] H. Nakazato, M. Namiki, and S. Pascazio, Int. J. Mod. Phys. B **10**, 247 (1996).

[27] P. Lambropoulos, G. M. Nikolopoulos, T. R. Nielsen, and S. Bay, Rep. Prog. Phys. **63**, 455 (2000).

[28] T. Petrosky, C.-O. Ting, and S. Garmon, Phys. Rev. Lett. **94**, 043601 (2005).

[29] S. Tanaka, S. Garmon, and T. Petrosky, Phys. Rev. B **73**, 115340 (2006).

[30] S. Longhi, Phys. Rev. Lett. **97**, 110402 (2006).

[31] D. Segal and D. R. Reichman, Phys. Rev. A **76**, 012109 (2007).

[32] S. Longhi, Phys. Rev. B **75**, 184306 (2007).

[33] H. Zheng, S. Y. Zhu, and M. S. Zubairy, Phys. Rev. Lett. **101**, 200404 (2008).

[34] W.-M. Zhang, P.-Y. Lo, H.-N. Xiong, M. W.-Y. Tu, and F. Nori, Phys. Rev. Lett. **109**, 170402 (2012).

[35] G. Engelhardt, G. Schaller, and T. Brandes, Phys. Rev. A **94**, 013608 (2016).

[36] T. Shi, Y.-H. Wu, A. González-Tudela, and J. I. Cirac, Phys. Rev. X **6**, 021027 (2016).

[37] Y. Liu and A. A. Houck, Nat. Phys. **13**, 48 (2017).

[38] S. Longhi, Int. J. Mod. Phys. B **31**, 1750249 (2017).

[39] R. Schmidt, M. Knap, D. A. Ivanov, J.-S. You, M. Cetina, and E. Demler, Rep. Prog. Phys. **81**, 024401 (2018).

[40] F. Schmidt, D. Mayer, Q. Bouton, D. Adam, T. Lausch, N. Spethmann, and A. Widera, Phys. Rev. Lett. **121**, 130403 (2018).

[41] A.-M. Visuri, C. Berthod, and T. Giamarchi, Phys. Rev. A **98**, 053607 (2018).

[42] R. G. Lena and A. J. Daley, Phys. Rev. A **101**, 033612 (2020).

[43] J. Mumford, W. Kirkby, and D. H. J. O' Dell, J. Phys. B: At., Mol. Opt. Phys. **53**, 145301 (2020).

[44] C. Cohen-Tannoudji, J. Dupont-Roc, and G. Grynberg, *Atom-Photon Interactions: Basic Processes and Applications* (Wiley, New York, 1998).

[45] N. Majlis, *The Quantum Theory of Magnetism* (World Scientific, New Jersey, 2007).

[46] C. Kittel, *Introduction to Solid State Physics* (Wiley, New York, 1953).

[47] D. Loss and D. P. Di Vincenzo, Phys. Rev. A **57**, 120 (1998).

[48] G. Burkard, D. Loss, and D. P. DiVincenzo, Phys. Rev. B **59**, 2070 (1999).

[49] M. A. Nielsen and I. L. Chuang, *Quantum Computation and Quantum Information* (Cambridge University Press, Cambridge, 2000).

[50] P. W. Shor, Phys. Rev. A **52**, R2493 (1995).

[51] A. Barenco, D. Deutsch, A. Ekert, and R. Jozsa, Phys. Rev. Lett. **74**, 4083 (1995).

[52] J. I. Cirac and P. Zoller, Phys. Rev. Lett. **74**, 4091 (1995).

[53] J. A. Jones, M. Mosca, and R. H. Hansen, Nature (London) **393**, 344 (1995).

[54] I. L. Chuang, N. Gershenfeld, and M. Kubinec, Phys. Rev. Lett. **80**, 3408 (1998).

[55] T. Holstein and H. Primakoff, Phys. Rev. **58**, 1098 (1940).

[56] H. E. Fettis, SIAM J. Math. Anal. **1**, 524 (1970).

[57] B. Misra and E. C. G. Sudarshan, J. Math. Phys. **18**, 756 (1977).

[58] D. Home and M. A. B. Whitaker, J. Phys. A: Math. Gen. **19**, 1847 (1986).

[59] W. M. Itano, D. J. Heinzen, J. J. Bollinger, and D. J. Wineland, Phys. Rev. A **41**, 2295 (1990).

[60] D. Home and M. A. B. Whitaker, Ann. Phys. (NY) **258**, 237 (1997).

[61] M. C. Fischer, B. Gutierrez-Medina, and M. G. Raizen, Phys. Rev. Lett. **87**, 040402 (2001).

[62] E. W. Streed, J. Mun, M. Boyd, G. K. Campbell, P. Medley, W. Ketterle, and D. E. Pritchard, Phys. Rev. Lett. **97**, 260402 (2006).

[63] G. A. Paz-Silva, A. T. Rezakhani, J. M. Dominy, and D. A. Lidar, Phys. Rev. Lett. **108**, 080501 (2012).

[64] W. Wu and H.-Q. Lin, Phys. Rev. A **95**, 042132 (2017).

[65] V. Debierre, I. Goessens, É. Brainis, and T. Durt, Phys. Rev. A **92**, 023825 (2015).

[66] L. Lerner, Phys. Rev. A **98**, 052132 (2018).

[67] P. Facchi and S. Pascazio, J. Phys. A: Math. Theor. **41**, 493001 (2008).

[68] P. Facchi, H. Nakazato, and S. Pascazio, Phys. Rev. Lett. **86**, 2699 (2001).

[69] A. G. Kofman and G. Kurizki, Nature (London) **405**, 546 (2000).

[70] J.-M. Zhang, J. Jing, L.-G. Wang, and S.-Y. Zhu, Phys. Rev. A **98**, 012135 (2018).